

On Uncertainty Quantification of Lithium-ion Batteries: Application to an $\text{LiC}_6/\text{LiCoO}_2$ cell

Mohammad Hadigol^a, Kurt Maute^a, Alireza Doostan^{a,*}

^a*Aerospace Engineering Sciences Department, University of Colorado, Boulder, CO 80309, USA*

Abstract

In this work, a stochastic, physics-based model for Lithium-ion batteries (LIBs) is presented in order to study the effects of parametric model uncertainties on the cell capacity, voltage, and concentrations. To this end, the proposed uncertainty quantification (UQ) approach, based on sparse polynomial chaos expansions, relies on a *small* number of battery simulations. Within this UQ framework, the identification of most important uncertainty sources is achieved by performing a global sensitivity analysis via computing the so-called Sobol' indices. Such information aids in designing more efficient and targeted quality control procedures, which consequently may result in reducing the LIB production cost. An $\text{LiC}_6/\text{LiCoO}_2$ cell with 19 uncertain parameters discharged at 0.25C, 1C and 4C rates is considered to study the performance and accuracy of the proposed UQ approach. The results suggest that, for the considered cell, the battery discharge rate is a key factor affecting not only the performance variability of the cell, but

*Corresponding Author: Alireza Doostan

Email addresses: mohammad.hadigol@colorado.edu (Mohammad Hadigol), maute@colorado.edu (Kurt Maute), alireza.doostan@colorado.edu (Alireza Doostan)

also the determination of most important random inputs.

Keywords: Lithium-ion battery; Uncertainty quantification; Polynomial chaos expansion; Compressive sampling; Global sensitivity analysis

1. Introduction

High energy and power densities of Lithium-ion batteries (LIBs) alongside their superior safety features have made them the number one energy storage device for a wide range of electric devices from cell phones to hybrid-electric vehicles and aerospace applications [1, 2, 3, 4]. Since the launch of the first commercial LIB in 1991 [5], significant work has been dedicated to modeling [6, 7, 8, 9, 10, 11], design optimization [12, 13, 14], and discovering new materials [15, 16, 17] for LIBs.

Among the proposed models for simulation of LIBs, the most widely used one is Newman's model [18, 6, 19], which is based on the porous electrode and concentrated solution theories. This model involves material and electrochemical properties, such as porosity of electrodes, solid particle size, and diffusion coefficients, which are measured/estimated directly or indirectly via experimental techniques [20]. Measurements of most physical quantities are accompanied by uncertainty due to accuracy limitations or natural, cell-to-cell variabilities. For example, measurements of the solid particle size in the LIB electrodes typically result in distributed values for the particle size [20, 21] rather than a single deterministic value which is mostly used in the LIB simulations. Performing additional measurements may lead to a better characterization of the solid particle size, but cannot completely eliminate the irreducible uncertainties due to natural variations. Hence, a deterministic treatment of the solid particle size may result in predictions

which do not agree with the experiments well. Consequently, LIB models which incorporate discrete or continuous particle size distributions have been developed [22, 23, 24, 25, 20]. Quantifying the impact of such uncertainties is essential for reliable model-based predictions, and is the focus of the emerging field of Uncertainty Quantification (UQ) in computational engineering and science. In general, UQ provides tools for assessing the credibility of model predictions and facilitating decision making under uncertainty [26, 27, 28]. UQ is also utilized for quantitative validation of simulation models [29, 30, 31] and robust design optimization under uncertainty [32, 33, 34].

One may represent the uncertain model parameters by random variables/processes. This is the subject of a major class of UQ approaches known as probabilistic techniques. Among these methods, stochastic spectral methods [35, 29] based on polynomial chaos (PC) expansions [36, 37] have received special attention due to their advantages over traditional UQ techniques such as perturbation-based and Monte Carlo sampling (MCS) methods. In particular, under certain regularity conditions, these schemes converge faster than MCS methods [38] and, unlike perturbation methods, are not restricted to problems with small uncertainty levels [35]. Stochastic spectral methods are based on expanding the solution of interest in PC bases. The coefficients of these expansions are then computed, for instance, intrusively via Galerkin projection [35], or non-intrusively via regression [39, 40, 41, 42] or quadrature integration [43]. For complex systems such as LIBs, non-intrusive methods are more attractive than intrusive ones since they allow the use of simulations as black boxes. In other words, there is no need to modify the available deterministic solvers when one uses non-intrusive PC expansions. In addition, since only independent solution realizations are needed, parallel imple-

mentation is straightforward.

Up to date, the majority of the LIB physics-based simulations have treated the underlying model parameters deterministically and ignored the effects of uncertainties in the model parameters on the performance of LIBs. There are a few works in the literature which have addressed the variability of LIB physics-based model parameters. In [20], PC expansion is employed within the Newman's model to demonstrate the reduction in the cell potentials as a result of the uncertainty in the particle size of the anode electrode. Effects of variability in cycling rate, particle size, diffusivity, and electrical conductivity of the cathode electrode on the LIB performance was examined in [44], where surrogate models are developed using the Newman's model together with techniques such as Kriging, polynomial response, and radial-basis neural networks. It was found that the randomness in electrical conductivity has the minimal effects on the cell performance, while the impact of the remaining parameters depend on the the cycling rate. In [45], impedance spectroscopy [46] is utilized to compare the relative importance of randomness in porosity, particle size, length and tortuosity of the cathode and separator using Nyquist stability criterion. It was shown that the particle size has the largest impact on the fluctuations in the impedance. In [47], a reduced order LIB model presented in [9] and a Bayesian inference technique are used to estimate the effective kinetic and transport parameters from experimental data. These works either employ a reduced order model of the LIB or only consider uncertainties in a few number of model parameters to avoid high computational costs.

This work presents a sampling-based PC approach to study the effects of uncertainty in various model parameters on the cell capacity, voltage, and concentrations of an LIB described by the Newman's model [18, 6, 19]. The proposed

PC approach, first introduced in [40], relies on the sparsity of expansion coefficients to accurately compute the statistics of quantities of interest with a small number of battery simulations. Through its application to an $\text{LiC}_6/\text{LiCoO}_2$ LIB model, we demonstrate that, unlike the previously mentioned works on UQ of LIBs, the proposed PC approach is capable of taking into account a large number of uncertain parameters. While the proposed PC-based UQ framework is general, the results we present are specific to the particular $\text{LiC}_6/\text{LiCoO}_2$ cell we consider and the choices of uncertainty models for its parameters. The latter are, as much as possible, identified from the reported experiments on identical or similar cells/materials.

Additionally, this UQ framework enables performing a global sensitivity analysis (SA) to identify the most important uncertain parameters affecting the variability of the output quantities. Such an analysis may be used toward reducing cell-to-cell variations and designing more efficient and targeted quality control procedures to reduce the manufacturing cost of LIBs [45, 48]. We also review the standard experimental techniques used for measuring the model parameters and discuss their impacts on the cell capacity and/or power.

It is worth highlighting that the present work is focused on modeling and propagation of parametric uncertainties, as opposed to model form uncertainties which may consider multiple competing models.

The remainder of this paper is organized as follows. Section 2 reviews the LIB model used in this study. In Section 3, we present our stochastic LIB modeling approach which is based on non-intrusive PC expansions. We then continue with reviewing a global sensitivity analysis approach via the Sobol' indices. Standard experimental techniques for measuring the model parameters and their underlying

distributions are discussed in Section 4. Finally, an $\text{LiC}_6/\text{LiCoO}_2$ cell is considered as our numerical example in Section 5.

2. LIB governing equations

An LIB schematic is presented in Fig. 1. During the discharge process, lithium ions in the solid particles of the anode diffuse to the particle surface where they oxidize into Li^+ ions and electrons and transfer to the electrolyte liquid (deintercalation). Electrons flow through the external circuit to the positive electrode. Meanwhile, Li^+ ions travel via diffusion and migration through the electrolyte and separator to the cathode where they are reduced and diffused into the solid particles (intercalation). When the LIB is charged, this process is reversed.

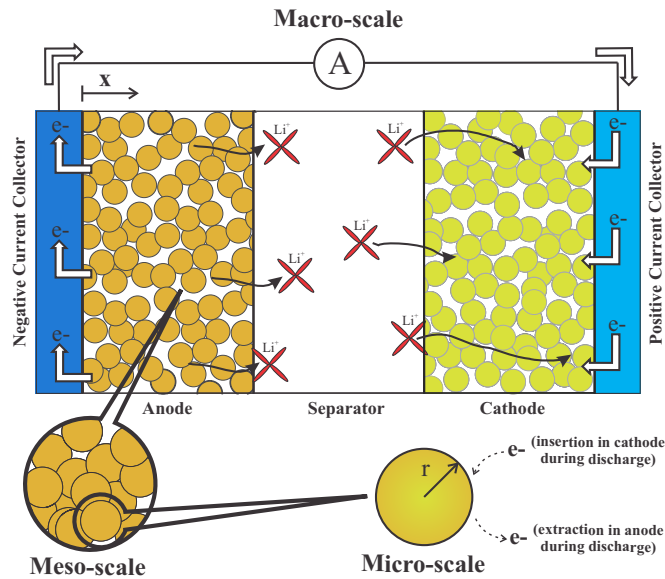


Figure 1: Schematic of a full cell LIB.

The Newman's LIB model is developed based on porous electrode and con-

concentrated solution theories [18, 6, 19]. The governing equations of this model for the salt concentration in liquid phase c , lithium concentration in solid phase c_s , liquid phase potential ϕ_e and solid phase potential ϕ_s are presented in Table 1. Symbols used in this table are defined in the nomenclature. The assumptions made in this model are summarized as: (i) transport properties are independent of temperature and simulations are isothermal; (ii) D , D_s and t_+^0 do not depend on the concentrations; (iii) volume changes within the cell are ignored; (iv) zero surface electrolyte inter-phase (SEI) resistance is considered; (v) no double layer capacitive effects are considered; and (vi) solid particles are spherical.

Table 1: Coupled non-linear governing equations of LIB.

	Governing equation	Boundary conditions
Electrolyte phase diffusion	$\frac{\partial(\epsilon c)}{\partial t} = \nabla(\epsilon D^{\text{eff}} \nabla c) + \frac{1-t_+^0}{F} j_{\text{vol}}$ (6)	$\nabla c _{x=0} = \nabla c _{x=L} = 0$
Solid phase diffusion	$\frac{\partial c_s}{\partial t} = \frac{1}{r^2} \frac{\partial}{\partial r} \left(D_s r^2 \frac{\partial c_s}{\partial r} \right)$ (7)	$\nabla c_s _{r=0} = 0$ $\nabla c_s _{r=r_s} = -\frac{j_{\text{vol}}}{aFD_s}$
Liquid phase potential	$\nabla(\kappa^{\text{eff}} \nabla \phi_e) - \nabla(\kappa_D^{\text{eff}} \nabla \ln c) + j_{\text{vol}} = 0$ (8)	$\nabla \phi_e _{x=0} = \nabla \phi_e _{x=L} = 0$ $\phi_e _{x=L} = 0$
Solid phase potential	$\nabla(\sigma^{\text{eff}} \nabla \phi_s) - j_{\text{vol}} = 0$ (9)	$\nabla \phi_s _{x=0} = \nabla \phi_s _{x=L} = \frac{-I}{\sigma^{\text{eff}}}$ $\nabla \phi_s _{x=L_a} = \nabla \phi_s _{x=L_a+L_s} = 0$
Reaction kinetics	$j_{\text{vol}} = ai_{\text{ex}} \left[\exp\left(\frac{0.5F\eta}{RT}\right) - \exp\left(-\frac{0.5F\eta}{RT}\right) \right]$ (10) $i_{\text{ex}} = Fk(c_s^{\text{surf}})^{0.5}(c_{s,\text{max}} - c_s^{\text{surf}})^{0.5}(c)^{0.5}$	

In the literature, numerical techniques such as finite difference [6], finite vol-

ume [49], and finite elements [50] have been used to solve this system of coupled non-linear equations simultaneously. In order to reduce the computational cost of the LIB simulations, using the concepts of particular and homogeneous solutions to Ordinary Differential Equations (ODEs), Reimers [51] suggested a decoupled formulation of Newman’s model, which we use in this study. For the sake of completeness, this decoupling technique is presented in Appendix A.

3. UQ via polynomial chaos expansion

Polynomial chaos expansion was first introduced by Wiener in 1938 [36]. It was reintroduced to the engineering field in 1991 by Ghanem and Spanos [35] for the problems with Gaussian input uncertainties and later extended to non-Gaussian random inputs by using the orthogonal polynomials of the Askey scheme (generalized PC expansion) [52]. PC expansion provides a framework to approximate the solution of a stochastic system by projecting it onto a basis of polynomials of the random inputs, which we review in the following.

Let $(\Omega, \mathcal{T}, \mathcal{P})$ be a complete probability space, where Ω is the sample set and \mathcal{P} is a probability measure on the σ -field \mathcal{T} . Also assume that the system input uncertainty has been discretized and approximated by random variables, such that the vector $\boldsymbol{\xi} = (\xi_1, \dots, \xi_d) : \Omega \rightarrow \mathbb{R}^d$, $d \in \mathbb{N}$, represents the set of independent random inputs. We also assume that probability density function (PDF) of the random variable ξ_k is denoted by $\rho(\xi_k)$, while $\rho(\boldsymbol{\xi})$ represents the joint PDF of $\boldsymbol{\xi}$. Let us assume that the finite variance output quantity of interest (QoI) defined on $(\Omega, \mathcal{T}, \mathcal{P})$ is denoted by $u(\boldsymbol{\xi})$. The truncated PC representation of $u(\boldsymbol{\xi})$, denoted by $\hat{u}(\boldsymbol{\xi})$, is

$$\hat{u}(\boldsymbol{\xi}) = \sum_{i \in \mathcal{I}_{d,p}} \alpha_i \psi_i(\boldsymbol{\xi}), \quad (11)$$

where α_i are the deterministic coefficients and $\psi_i(\boldsymbol{\xi})$ are the multivariate PC basis functions. The basis functions $\psi_i(\boldsymbol{\xi})$ in (11) are generated from

$$\psi_{\mathbf{i}}(\boldsymbol{\xi}) = \prod_{k=1}^d \psi_{i_k}(\xi_k), \quad \mathbf{i} \in \mathcal{I}_{d,p}, \quad (12)$$

where $\psi_{i_k}(\xi_k)$, $k = 1, \dots, d$, are univariate polynomials of degree $i_k \in \mathbb{N}_0 := \mathbb{N} \cup \{0\}$ orthogonal with respect to $\rho(\xi_k)$ (see, e.g., Table 2), i.e.,

$$\mathbb{E}[\psi_{i_k} \psi_{j_k}] = \int \psi_{i_k}(\xi_k) \psi_{j_k}(\xi_k) \rho(\xi_k) d\xi_k = \delta_{i_k j_k} \mathbb{E}[\psi_{i_k}^2], \quad (13)$$

where $\delta_{i_k j_k}$ is the Kronecker delta and $\mathbb{E}[\cdot]$ denotes the mathematical expectation operator. The multi-index \mathbf{i} in (11) is $\mathbf{i} = (i_1, \dots, i_d) \in \mathcal{I}_{d,p}$ and the set of multi-indices $\mathcal{I}_{d,p}$ is defined by

$$\mathcal{I}_{d,p} = \{\mathbf{i} = (i_1, \dots, i_d) \in \mathbb{N}_0^d : \|\mathbf{i}\|_1 \leq p\}, \quad (14)$$

where $\|\cdot\|_1$ is the l_1 norm and the size of $\mathcal{I}_{d,p}$, hence the number P of PC basis functions of total order not larger than p in dimension d , is given by

$$P = |\mathcal{I}_{d,p}| = \frac{(p+d)!}{p!d!}. \quad (15)$$

Due to the orthogonality of the polynomials $\psi_{i_k}(\xi_k)$ and given that the ξ_k are independent, the PC basis functions $\psi_{\mathbf{i}}(\boldsymbol{\xi})$ are also orthogonal, i.e., $\mathbb{E}[\psi_{\mathbf{i}} \psi_{\mathbf{j}}] = \delta_{\mathbf{i}, \mathbf{j}} \mathbb{E}[\psi_{\mathbf{i}}^2]$. The truncated PC expansion in (11) converges in the mean-square sense as $p \rightarrow \infty$ when $u(\boldsymbol{\xi})$ has finite variance and the coefficients α_i are computed from the projection equation $\alpha_i = \mathbb{E}[u(\cdot) \psi_i(\cdot)] / \mathbb{E}[\psi_i^2]$ [52]. For convenience, we also index the PC basis functions by $\{1, \dots, P\}$ so that there is a one-to-one correspondence between $\{\psi_j(\boldsymbol{\xi})\}_{j=1}^P$ and $\{\psi_{\mathbf{i}}(\boldsymbol{\xi})\}_{\mathbf{i} \in \mathcal{I}_{d,p}}$.

Table 2: Correspondence of Wiener-Askey polynomial chaos and probability distribution of the random variables [52].

$\rho(\xi_k)$	Polynomial type	Support
Gaussian	Hermite	$(-\infty, +\infty)$
Gamma	Laguerre	$(0, +\infty)$
Beta	Jacobi	$[a, b]$
Uniform	Legendre	$[a, b]$

3.1. Non-intrusive polynomial chaos expansion

The main task in PC-based methods is to compute the coefficients of the solution expansion either intrusively [35] or non-intrusively [53]. In an intrusive approach, the governing equations are projected onto the subspace spanned by the PC basis via the Galerkin formulation. The final system of equations to be solved in an intrusive PC expansion method is P times larger than the size of the deterministic counterpart. This approach may require some modifications of the existing deterministic solvers, which for complex problems such as LIBs, may be difficult and time-consuming to implement. On the other hand, non-intrusive methods facilitate the use of existing deterministic solvers and treat them as a black box. The first task is to generate a set of N deterministic or random samples of $\boldsymbol{\xi}$, denoted by $\{\boldsymbol{\xi}^{(i)}\}_{i=1}^N$. Next, corresponding to these samples, N realizations of the output QoI, $\{u(\boldsymbol{\xi}^{(i)})\}_{i=1}^N$, are computed using an available deterministic solver. The last step is solving for the PC coefficients using these realizations. Several methods such as least squares regression [39], pseudo-spectral collocation [29], Monte Carlo sampling [38], and compressive sampling (CS) [40] have

been employed in the literature for this purpose. Once the PC coefficients are computed, the mean, $\mathbb{E}[\cdot]$, and variance, $\text{var}[\cdot]$, of $u(\boldsymbol{\xi})$ can be directly approximated by

$$\mathbb{E}[\hat{u}] = \alpha_0, \quad (16)$$

and

$$\text{var}[\hat{u}] = \sum_{\substack{i \in \mathcal{I}_{d,p} \\ i \neq 0}} \alpha_i^2. \quad (17)$$

In the following, we will review the least squares regression and the compressive sampling methods.

3.1.1. Least squares regression

The least squares regression technique is basically the regression of the exact solution $u(\boldsymbol{\xi})$ in the PC bases [54]. Given the set of samples $\{\boldsymbol{\xi}^{(i)}\}_{i=1}^N$, generated randomly, for instance, according to $\rho(\boldsymbol{\xi})$, and the corresponding solution realizations $\{u(\boldsymbol{\xi}^{(i)})\}_{i=1}^N$, the discrete representation of (11) can be written as

$$\boldsymbol{\Psi}\boldsymbol{\alpha} \approx \boldsymbol{u}, \quad (18)$$

where $\boldsymbol{u} = (u(\boldsymbol{\xi}^{(1)}), \dots, u(\boldsymbol{\xi}^{(N)}))^T \in \mathbb{R}^N$ contains the realizations of the QoI, $\boldsymbol{\Psi}(i, j) = \psi_j(\boldsymbol{\xi}^{(i)}) \in \mathbb{R}^{N \times P}$ is the measurement matrix containing samples of the PC basis, and $\boldsymbol{\alpha} = (\alpha_1, \dots, \alpha_P)^T \in \mathbb{R}^P$ is the vector of PC coefficients.

PC coefficients may be approximated by solving the least squares problem

$$\min_{\boldsymbol{\alpha}} \|\boldsymbol{u} - \boldsymbol{\Psi}\boldsymbol{\alpha}\|_2, \quad (19)$$

where $\|\cdot\|_2$ is the l_2 norm. When $\boldsymbol{\Psi}$ is full rank, the solution to (19) is computed from the normal equation

$$(\boldsymbol{\Psi}^T \boldsymbol{\Psi})\boldsymbol{\alpha} = \boldsymbol{\Psi}^T \boldsymbol{u}. \quad (20)$$

In general, a stable solution α to (20) requires $N > P$ realizations of $u(\xi)$. In [42, Theorems 2.2 and 3.1], it is shown that for d -dimensional Legendre polynomials of total order p , for the case of $d > p$, a stable solution recovery from (19) can be guaranteed with a number of samples given by

$$N \geq 3^p C P \log(P), \quad (21)$$

where C is an absolute constant. This suggests that the number of samples N depends linearly on P (up to a logarithmic factor) for the least squares regression method.

For high dimensional complex problems, such as LIBs, generating $N > P$ realizations may be computationally expensive. In such cases, when the solution $u(\xi)$ depends *smoothly* on ξ , the PC coefficients are often sparse, i.e., many of them are negligible. In these cases, CS may be employed to compute the coefficients with $N < P$ realizations [40, 42, 55, 41, 56, 57, 58, 59]. Specifically, the importance sampling approach of [41] ensures an accurate computation of α with a number of solution realizations that depends linearly (up to a logarithmic factor in P) on the number of dominant coefficients. We next review the CS approach, which we use later for the UQ of LIBs.

3.1.2. Compressive sampling

Compressive sampling/sensing is an emerging direction in signal processing which enables (up to) exact reconstruction of signals admitting sparse representations with a small number of signal measurements [60, 61, 62]. It was first introduced to the UQ field in 2011 by Doostan and Owhadi [40] where they used CS to approximate sparse PC solutions to stochastic PDEs. The main requirement in CS methods is to have a sparse solution at the stochastic level, that is a small

fraction of PC coefficients in (11) are dominant and contribute to the solution statistics. The ultimate goal of CS is to approximate the sparse PC coefficients α accurately and robustly with $N < P$ realizations of $u(\boldsymbol{\xi})$.

With $N < P$, the underdetermined linear system in (18) is ill-posed and generally has infinitely many solutions. Sparsity of the PC coefficients α allows a regularization of (18) to ensure a well-posed solution [40]. This can be achieved by solving the Basis Pursuit Denoising (BPDN) problem

$$\min_{\alpha} \|\alpha\|_1 \quad \text{subject to} \quad \|\Psi\alpha - \mathbf{u}\|_2 \leq \gamma. \quad (22)$$

Minimization of the l_1 norm in (22) promotes sparsity in α , while the l_2 residual norm controls the accuracy of the truncated PC expansion with the tolerance γ . Several numerical techniques are available in the literature to solve the BPDN problem [40]. Among those, we adopt the Spectral Projected Gradient algorithm (SPGL1) of [63] implemented in the `SPGL1` package for MATLAB [64].

The accuracy of α computed from (22) depends on the sample size N and the truncation error $\|\Psi\alpha - \mathbf{u}\|_2$ in (22). In general, the truncation error may be decreased by increasing the order p of the PC basis, which leads to a larger number of coefficients, P . This, in turn, requires a larger number of samples N to maintain the stability of the BPDN problem. The minimum sampling rate depends on the type of the PC basis, the sparsity of α , and the sampling distribution according to which $\{\boldsymbol{\xi}^{(i)}\}_{i=1}^N$ are generated, and is shown to linearly depend on the number of dominant PC coefficients [41, Theorems 3.1 and 4.2]. More precisely, for d -dimensional Legendre polynomials of total order p , where $d > p$, the number of samples N required to guarantee a stable solution recovery from (22) is given by

$$N \geq 3^p C S \log(P), \quad (23)$$

where S is the number of dominant coefficients. In (23), N depends primarily on S and weakly on P through the $\log(P)$ term. For high dimensional complex problems, we usually have $P \gg S$, hence, a comparison of (21) and (23) suggests that the CS approach requires considerably smaller number of samples in comparison to the least squares regression.

In practice, one may start by approximating a lower order PC expansion when N is small and increase p when a larger number of samples become available. Another important factor in the sparse reconstruction is the selection of the truncation error tolerance γ . The ideal value for the tolerance is $\gamma \approx \|\Psi\alpha_{\text{exact}} - \mathbf{u}\|_2$. Since the exact PC coefficients α_{exact} are not known, selecting larger values than $\|\Psi\alpha_{\text{exact}} - \mathbf{u}\|_2$ for γ deteriorates the accuracy of the approximation, while smaller choices may result in over-fitting the solution samples and, thus, less accurate results. In the numerical results of Section 5, we employ the cross-validation approach in [40, Section 3.5] to optimally choose γ . For the sake of completeness, this cross-validation approach is summarized in Algorithm 1. For more details about the CS method, the interested reader is referred to [40, 41].

Algorithm 1 Algorithm for cross-validation estimation of γ .

- 1: Divide the N solution samples to N_r reconstruction and N_v validation samples.
 - 2: Choose multiple values for γ_r such that the exact truncation error $\|\Psi\alpha_{\text{exact}} - \mathbf{u}\|_2$ of the reconstruction samples is within the range of γ_r values.
 - 3: For each value of γ_r solve the BPDN problem (22) using the N_r reconstruction samples to compute α_r .
 - 4: For each value of γ_r , compute the truncation error $\gamma_v := \|\Psi_v\alpha_r - \mathbf{u}_v\|_2$ of the N_v validation samples.
 - 5: Find the minimum value of γ_v and its corresponding $\hat{\gamma}_r := \gamma_r$.
 - 6: Set $\gamma = \sqrt{\frac{N}{N_r}\hat{\gamma}_r}$.
-

3.2. Global sensitivity analysis

Identification of the most important random inputs affecting the variations in the cell voltage, capacity, and concentrations is one of the objectives of this study. This is achieved by performing a global sensitivity analysis (SA) to quantify the specific effects of random inputs on the variance of the QoI.

Among the available techniques to perform global SA, we use the Sobol' indices [65] which are widely used due to their generality and accuracy. Sudret [54] introduced an analytic approach to compute the Sobol' indices as a post-processing of the PC coefficients. Let us assume the PC coefficients in (11) are computed. The first order PC-based Sobol' index S_k , which represents the sole effects of the random input ξ_k on the variability of $u(\boldsymbol{\xi})$, is given by

$$S_k = \sum_{i \in \mathcal{I}_k} \alpha_i^2 / \text{var}[u], \quad \mathcal{I}_k = \{\mathbf{i} \in \mathbb{N}_0^d : i_k > 0, i_{m \neq k} = 0\}, \quad (24)$$

where $\text{var}[u]$ is given in (17). In computing S_k , it is assumed that all random inputs except ξ_k are fixed, therefore, S_k does not represent the effects of the interactions between ξ_k and other random inputs. In order to quantify the total effects of the random input ξ_k , including the interactions between random inputs on the variability of $u(\boldsymbol{\xi})$, one needs to compute the total PC-based Sobol' indices defined as

$$S_k^T = \sum_{\mathbf{i} \in \mathcal{J}_k^T} \alpha_{\mathbf{i}}^2 / \text{var}[u], \quad \mathcal{J}_k^T = \{\mathbf{i} \in \mathbb{N}_0^d : i_k > 0\}. \quad (25)$$

The smaller S_k^T , the less important random input ξ_k . For the cases when $S_k^T \ll 1$, ξ_k is considered as insignificant and may be replaced by its mean value without considerable effects on the variability of $u(\boldsymbol{\xi})$. In this study, we employ S_k^T as a measure to identify the most important random inputs of the LIB model considered.

4. Uncertainty in LIB model parameters

The model parameters of LIBs are measured experimentally and are accompanied by uncertainty due to natural or experimental variability. Some of these parameters are measured using complex electrochemical techniques, while others are obtained via simple experiments. In the following, we will discuss a number of such techniques. It should be noted that because of the limited data available in the literature, we could not avoid making assumptions on the probability distribution for some of the parameters. Additionally, the reported uncertainty models are specific to the LiC₆/LiCoO₂ cell we consider here.

4.1. Porosity, ϵ

Porosity is defined as the ratio of the pore volume to the bulk volume. Manufacturers choose the porosity as a trade off between power and energy, i.e., the higher the porosity, the higher the power and the lower the capacity [66]. There are several methods to measure the porosity, such as the Method of Standard Porosimetry (MSP) [67], porosity measurement using liquid or gas absorption methods according to the American Society for Testing and Materials (ASTM) D-2873 [68], and X-ray tomography [69].

In [45], a uniform distribution [0.28, 0.32] is considered for the porosity of LiCoO_2 based on experimental data, which has $\pm 6.7\%$ (of the mean) variation around the mean. DuBeshter et al. [67] reported $\pm 4.5\%$ variability for porosity of the graphite anode electrode, while a higher value of $\pm 12.6\%$ is reported for the separator. Hence, in the present study, we assume a uniform distribution for the porosity with $\pm 6.7\%$, $\pm 4.5\%$, and $\pm 12.6\%$ variation around the mean in LiCoO_2 cathode, LiC_6 anode, and separator, respectively. Defining the coefficient of variation (COV) as the ratio of the standard deviation to the mean, the assumed variations translate to COVs of 0.026, 0.073, and 0.038 in anode, separator, and cathode, respectively.

4.2. Solid particle size, r_s

The flux of Li^+ at the electrode-electrolyte interface is affected by the solid particle size in electrodes, as it defines the available surface area for the reaction. The maximum battery power may be increased by decreasing the particle size of the electrode material and increasing the surface area per volume.

The particle size distribution may be measured by a laser diffraction and scattering device [70], X-ray computed tomography (XCT) [71], or focused ion beam

tomography [72].

Santhanagopalan and White [20] considered a normal distribution for a graphite anode with the mean and standard deviation of $6.2 \mu\text{m}$ and $0.42 \mu\text{m}$, respectively, to quantify the effects of random particle size. For the particle size distribution of LiCoO_2 , a normal distribution with mean of $7.7 \mu\text{m}$ and standard deviation of approximately $1.5 \mu\text{m}$ is reported in [21]. The corresponding COV values are 0.0677 and 0.1948 for the graphite anode and LiCoO_2 cathode, respectively. Nominal values, i.e., mean, of the particle sizes in both electrodes are equal to $2.0 \mu\text{m}$ in our cell. Because of the limited data available in the literature on the particle size distribution of our specific electrodes, we use these COVs to find the corresponding standard deviations. Based on these COVs, we assume a normal distribution with a mean of $2.0 \mu\text{m}$ and standard deviation of $0.1354 \mu\text{m}$ for the graphite anode. For the cathode electrode, the same mean value but a standard deviation of $0.3896 \mu\text{m}$ is considered.

Remark 1. *When one draws samples from a Gaussian distribution for the solid particle size r_s , one should assure that all the r_s samples are strictly positive. For this purpose, we here employed a truncated Gaussian distribution bounded between mean ± 3 standard deviation of r_s .*

4.3. Bruggeman coefficient, brugg

In porous electrode theory, instead of specifying the exact position and shapes of all pores and particles, a volume-averaged formulation is used [5]. In this model, the effective transport properties of the liquid phase, D^{eff} and κ^{eff} , are obtained using the porosity ϵ and tortuosity τ via

$$\kappa^{\text{eff}} = \frac{\epsilon\kappa}{\tau}, \quad D^{\text{eff}} = \frac{\epsilon D}{\tau}. \quad (26)$$

Tortuosity τ is a geometric parameter and depends on the porous electrode structure [73]. Although in recent years researchers have attempted to measure τ via experimental techniques [73, 74, 67, 66], because of the experimental complexities, τ has been commonly used as a model parameter that is calibrated by experiments [19]. More precisely, τ is computed via the well-known Bruggeman relation

$$\tau = \epsilon^{(1-\text{brugg})}, \quad (27)$$

where the Bruggeman exponent brugg is chosen to match numerical results with experimental data, and is usually assumed to be 1.5 [73].

Since the Bruggeman relation is widely used in LIB simulations, instead of taking τ as a random input parameter, we choose the Bruggeman exponent brugg to be an uncertain parameter in determining the effective properties. In [67], a uniform distribution with $\pm 4.9\%$ of the mean variation around the mean is reported for the Bruggeman exponent of the LiC_6 anode, while $\pm 33.3\%$ is considered for the Bruggeman exponent in separator brugg_s [45]. For this study, we assume a uniform distribution for the Bruggeman exponent with $\pm 5.0\%$ variations around the mean in both electrodes and $\pm 20.0\%$ in separator, which corresponds to COVs of 0.029 and 0.115, respectively.

4.4. Li^+ transference number, t_+^0

When an LIB is discharged, electrolyte salt dissociates into Li^+ and PF_6^- ions. The portion of the current that is carried by Li^+ ions is called the Li^+ transference number. The higher the Li^+ transport number, the higher the battery power [75].

Hittorf’s method [76], ac impedance spectroscopy [77], or pulsed field gradient NMR (pfg-NMR) technique [78] are used to measure the transference number in electrolytes. The experimental error of pfg-NMR technique for binary solutions is estimated to be around 5.0% [79]. Hence, we let the transference number uniformly change between 0.345 and 0.381 in this study.

4.5. Salt diffusion coefficient in the liquid phase, D

The salt diffusion coefficient D is a measure of the friction forces between the ions and the solvents [80]. In order to restrict the performance-limiting salt concentration gradients, which form in the electrolyte during polarization, it is critical to have a high salt diffusion coefficient [81]. High values of D lead to higher battery power. Experimental methods such as cyclic voltammetry (CV) [82] and electrochemical impedance spectroscopy (EIS) [83] have been used to measure D .

Salt diffusion coefficient is usually reported as a constant, but in [79] it is assumed to be a function of temperature and salt concentration. In this study, we assume a uniform distribution for D with $\pm 10.0\%$ variation around the mean, which corresponds to COV of 0.0577.

4.6. Diffusion coefficient of the solid, D_s

Diffusion coefficient of the solid phase plays an important role in the performance of LIBs since it affects the intercalation flux. Electrochemical techniques such as CV, GITT and EIS have been used to determine D_s [84]. D_s has been mostly treated as a constant value in LIB simulations [12], while it has been shown that D_s depends on the intercalation level, i.e., the ratio of $c_s^{\text{surf}}/c_{s,\text{max}}$ [85]. The values of D_s for the same materials, reported by different research groups, may

differ by several orders of magnitude. These large differences may suggest that a Fickian diffusion model which is used to calibrate D_s does not correctly describe the transport of Lithium within the active particles and other transport models need to be considered.

In this study, we assume that D_s does not depend on the intercalation level. Hence, for D_s , we assume a uniform distribution with the same COV we assumed for D .

4.7. Electronic conductivity of the solid, σ

Capacity of LIBs may be improved by increasing the solid phase electronic conductivity by using conductive additives in the electrode materials [86]. Two-point and four-point probe techniques have been used to measure the electronic conductivity of electrode materials [87]. Although σ depends on temperature and state of the charge [88], it is mostly treated as a constant in LIB simulations.

Reported values of σ in the literature for LiC_6 anode are mostly around $100 \text{ S} \cdot \text{m}^{-1}$ [9, 2, 12], while the electronic conductivity of LiCoO_2 cathode is reported to be $100 \text{ S} \cdot \text{m}^{-1}$ [9] and $10 \text{ S} \cdot \text{m}^{-1}$ [2]. In our LIB model, the nominal values of σ is equal to $100 \text{ S} \cdot \text{m}^{-1}$ for both electrodes. Because of the limited available data in the literature on the measurement uncertainties in σ , we assume that in both electrodes it changes uniformly with $\pm 10.0\%$ variation.

4.8. Reaction rate constant, k

Exchange current density i_{ex} is measured at the initial state of the battery [89]. Using the relation $i_{ex} = Fk(c_s^{\text{surf}})^{0.5}(c_{s,max} - c_s^{\text{surf}})^{0.5}(c)^{0.5}$, one can calculate the reaction rate constant k for each electrode at the initial values of c_s^{surf} and c . Although k shows an Arrhenius type dependence on temperature and depends on

the nature of the electrode surface [90], it is usually treated as a constant in LIB simulations. Higher reaction rate constants are favored for Li-ion batteries since the reaction is more reversible, and polarization effects are lower.

Because of the lack of experimental data on the reaction rate constant, we assumed that k has a uniform distribution with $\pm 10.0\%$ variation around the mean in both electrodes.

A list of random parameters considered in this study is presented in Table 3. In addition to the discussed input parameters, we also took the lengths L of electrodes and separator to be random in order to study the effect of uncertainties in geometrical parameters of the battery. It also should be noted that in our battery model, the effective ionic conductivity of the liquid phase κ^{eff} is considered to be a function of liquid concentration. Hence, κ^{eff} will be automatically a random parameter since the porosity is considered to be random. We note that the anodic and cathodic transfer coefficients (considered to be 0.5 in this study) as well as the open circuit potentials are also subjected to uncertainties; however, we treat them as deterministic parameters in this study.

Table 3: List of random and deterministic LIB inputs used in this study.

Random Input	Nominal Value	Distribution
$r_{s,a}$ [μm]	2	Gaussian, $\mu = 2, \sigma = 0.1354$
$r_{s,c}$ [μm]	2	Gaussian, $\mu = 2, \sigma = 0.3896$
ϵ_a	0.485	Uniform, [0.46, 0.51]
ϵ_s	0.724	Uniform, [0.63, 0.81]
ϵ_c	0.385	Uniform, [0.36, 0.41]
brugg_a	4	Uniform, [3.8, 4.2]
brugg_s	4	Uniform, [3.2, 4.8]
brugg_c	4	Uniform, [3.8, 4.2]
t_+^0	0.363	Uniform, [0.345, 0.381]
D [$\text{m}^2 \cdot \text{s}^{-1}$]	7.5×10^{-10}	Uniform, $[6.75, 8.25] \times 10^{-10}$
$D_{s,a}$ [$\text{m}^2 \cdot \text{s}^{-1}$]	3.9×10^{-14}	Uniform, $[3.51, 4.29] \times 10^{-14}$
$D_{s,c}$ [$\text{m}^2 \cdot \text{s}^{-1}$]	1×10^{-14}	Uniform, $[0.9, 1.1] \times 10^{-14}$
σ_a [$\text{S} \cdot \text{m}^{-1}$]	100	Uniform, [90, 110]
σ_c [$\text{S} \cdot \text{m}^{-1}$]	100	Uniform, [90, 110]
k_a [$\text{m}^4 \cdot \text{mol} \cdot \text{s}$]	5.03×10^{-11}	Uniform, $[4.52, 5.53] \times 10^{-11}$
k_c [$\text{m}^4 \cdot \text{mol} \cdot \text{s}$]	2.334×10^{-11}	Uniform, $[2.10, 2.56] \times 10^{-11}$
L_a [μm]	80	Uniform, [77, 83]
L_s [μm]	25	Uniform, [22, 28]
L_c [μm]	88	Uniform, [85, 91]

5. Numerical Example

In this section, we present a numerical example to demonstrate the application of our proposed UQ approach to LIBs. The one-dimensional $\text{LiC}_6/\text{LiCoO}_2$ cell we consider here is studied in [9]. We present our results for three different discharge rates of 0.25C, 1C, and 4C to study its effects on the propagation of uncertainty. We note that assuming a constant discharge rate is an idealized scenario. Typically, the battery loading varies over the course of the discharge process, depending on an application-dependent usage of the battery. Hence, in addition to the previously mentioned uncertain parameters, the discharge rate should also be considered as an uncertain input for the LIB model. For the sake of comparison, we treat the discharge rate as a deterministic input in this study, while our proposed UQ framework can incorporate random discharge rates with no difficulties, perhaps, with a cost of running additional battery simulations.

For the spatial discretization of the LIB governing equations, we used the Finite Difference Method on the non-uniform grids described in [51]. We also performed a mesh convergence analysis to ensure that spatial discretization errors are inconsequential.

Remark 2. *Working with a fine mesh and a small time step is advised when one employs sampling-based UQ techniques since a coarse discretization may not return a converged/accurate solution for all samples. In our calculations, we found that having 120 non-uniform grid points in each region and 26 non-uniform grid points in the spherical solid particles are sufficient to obtain accurate realizations for all of the samples. Moreover, constant time steps of 1.0, 0.1, and 0.05 seconds were used for 0.25C, 1C, and 4C rates of discharge, respectively.*

The cell model incorporating the nominal values in Table 3 is referred to as the *deterministic* model, while the *stochastic* model uses the distributed input parameters of Table 3. The number of random inputs of our stochastic LIB model is $d = 19$, which may be considered *high*. We use the CS technique in this study to approximate the sparse PC coefficients since, in comparison to least squares regression, CS requires smaller number of battery simulations.

Having at hand a deterministic LIB solver, the next step in sampling-based PC expansion is to generate N realizations of model parameters listed in Table 3. To this end, we assign an independent random variable ξ_k , $k = 1, \dots, d$, to each parameter, and consider an appropriate linear transformation of each ξ_k to match the PDF of the corresponding parameter in Table 3. For Gaussian and uniform PDFs, we use ξ_k 's that are standard Gaussians and uniformly distributed between $[-1, 1]$, respectively. The independent samples of $\boldsymbol{\xi}$, i.e., $\{\boldsymbol{\xi}^{(i)}\}_{i=1}^N$, are used to generate N independent samples of the model parameters, for which the LIB model is simulated to obtain N realizations of the output QoIs, $\{u(\boldsymbol{\xi}^{(i)})\}_{i=1}^N$. In our numerical experiments, we simulate each battery realization until a cut-off potential of 2.8 V is reached. Then using $\{\boldsymbol{\xi}^{(i)}\}_{i=1}^N$ and $\{u(\boldsymbol{\xi}^{(i)})\}_{i=1}^N$, we solve the BPDN problem in (22) to approximate the vector of PC coefficients $\boldsymbol{\alpha}$. These in turn will be used to compute the statistics of $u(\boldsymbol{\xi})$, such as the mean and variance given in (16) and (17), respectively, as well as the total Sobol' indices defined in (25).

We find that a PC expansion of order $p = 3$ and $N = 1000$ battery simulations are needed to achieve a *validation error* smaller than 1.0% as specified next. Following the cross-validation procedure described in [40, Section 3.5], we divide the $N = 1000$ samples into $N_r = 900$ reconstruction and $N_v = 100$ validation

samples to estimate the optimum value of γ in (22), using which we compute the solution α from (22). To verify the accuracy of the resulting PC expansion, we compute the validation error

$$\text{relative error} = \frac{\|\mathbf{u}_v - \Psi_v \alpha_r\|_2}{\|\mathbf{u}_v\|_2}, \quad (28)$$

where \mathbf{u}_v is the vector of $N_v = 1000$ additional realizations of QoI (not used in computing α) and Ψ_v is the measurement matrix corresponding to \mathbf{u}_v . Stated differently, the error in (28) determines the accuracy of constructed PC model in predicting independent QoI realizations. In practice, there is no need to generate additional samples for validation and we only used a larger number of validation samples to demonstrate the accuracy and robustness of our proposed method.

Remark 3. *In practice, we rely on the validation error to estimate the solution accuracy and decide to possibly increase the total order of PC expansion p . When the validation error does not reduce by increasing the number of numerically generated LIB samples for a given expansion order p , one may achieve smaller validation errors by increasing p with a cost of increased number of LIB simulations.*

Algorithm 2 summarizes the main steps in our proposed UQ framework for LIBs for a fixed PC expansion order p .

Algorithm 2 Summary of the main steps in the proposed UQ framework for LIBs.

- 1: Identify uncertain parameters and their probability distributions (Section 4).
 - 2: **while** the validation error in (28) is larger than a user-defined threshold **do**
 - 3: Generate N realizations of the uncertain parameters based on their PDFs.
 - 4: Perform deterministic LIB simulations to obtain the output QoI (Section 2).
 - 5: Evaluate the corresponding realization of the PC basis (Section 3.1).
 - 6: Perform the cross-validation approach in Algorithm 1 to optimally estimate δ .
 - 7: Solve the BPDN problem in (22) to approximate the PC coefficients.
 - 8: Increase N .
 - 9: **end while**
 - 10: Compute the statistics of the output QoI via (16) and (17) and the total Sobol' indices via (25).
-

5.1. Results

5.1.1. Effects of input uncertainties on cell capacity

Capacity is defined as the available energy stored in a fully charged LIB and is one of the most important factors affecting the battery performance. However, effects of LIB model uncertainties on capacity estimation are not yet fully explored.

Fig. 2 demonstrates the effects of LIB model uncertainties in estimating the cell capacity. In Fig. 2(a), cell capacities as a function of the cell voltage obtained from deterministic and stochastic models are presented for 0.25C, 1C and 4C rates of galvanostatic discharge. Shaded areas around the mean of stochastic cell capacity represent three standard deviation intervals. As it can be seen, noticeable

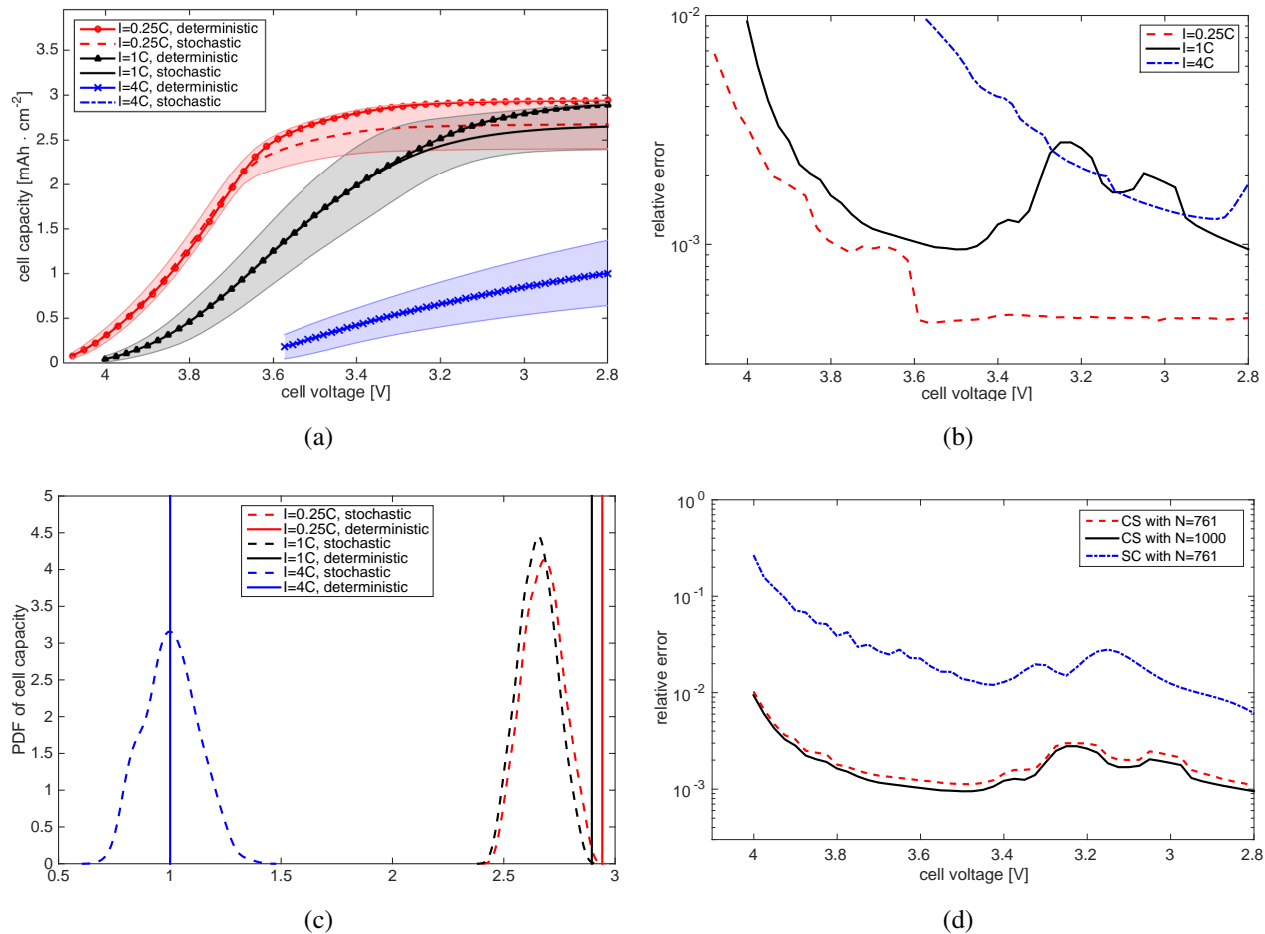


Figure 2: Comparison of stochastic and deterministic battery models for $I = 0.25C$, $1C$ and $4C$ rates of galvanostatic discharge. (a) Stochastic and deterministic cell capacities as a function of the cell voltage. The shaded areas are probability bounds of three standard deviations around the mean; (b) Relative error as a function of the cell voltage; (c) PDFs of the cell capacity; (d) Comparison of the relative error obtained by the CS method and the level two SC technique on a Clenshaw-Curtis grid [91] for $1C$ rate of discharge. Level three SC method requires 9976 LIB simulations.

deviation from the deterministic capacity starts when the cell voltage experiences a rapid drop-off. As the discharge rate is decreased, the onset of this deviation happens at higher cell voltages, i.e., at $\phi_{\text{cell}} \approx 3.7$ V for $I = 0.25\text{C}$ and $\phi_{\text{cell}} \approx 3.3$ V for $I = 1\text{C}$. This plot shows that for low to medium rates of discharge, a deterministic simulation of LIB overestimates the cell capacity. For 4C discharge rate, the mean of stochastic cell capacity overlaps with the cell capacity predicted by the deterministic model. One may suspect that at high discharge rates, input uncertainties have no significant effect on the cell capacity, but the probability bounds around the mean of cell voltage for $I = 4\text{C}$ suggest otherwise. As it can be seen, the largest standard deviation of the cell capacity at the end of discharge is for the 4C discharge rate.

Fig. 2(b) shows the validation error in approximating the PC coefficients of the cell capacity. With $p = 3$ and $d = 19$, the number of PC coefficients $P = |\mathcal{S}_{19,3}| = 1540$, which is larger than $N = 1000$. The accurate solution approximation in this under-sampled setting is achieved by minimizing the l_1 norm of α in the BPDN problem (22).

A comparison of deterministic (solid line) and distributed (dashed line) cell capacities is also presented in Fig. 2(c). This plot suggests that the probability of achieving deterministic cell capacity when the cell is subjected to assumed input uncertainties is very small for low to medium discharge rates, while this probability is considerably larger for higher discharge rates.

An alternative sampling-based approach to compute the PC coefficients is the stochastic collocation (SC) method [92, 93, 94]. The main idea behind the SC technique is to sample the output QoI at particular points in the stochastic space and then approximate the solution via interpolation or the solution statistics by

numerical integration. For high-dimensional problems, sparse tensor products first introduced by Smolyak [95], which may be built upon the Clenshaw-Curtis abscissas, has been proposed to relax the *curse-of-dimensionality* associated with full tensor products [91]. The accuracy of this method is controlled by the so-called level parameter. The number of required LIB simulations increases with the magnitude of the level parameter. SC may also be used to compute the PC coefficients via the projection equation $\alpha_i = \mathbb{E}[u(\cdot)\psi_i(\cdot)]/\mathbb{E}[\psi_i^2]$. In particular, the numerator in this equation is a d -dimensional integral over Ω which may be computed using tensor product quadrature or cubature rules. Detailed description of these techniques is beyond the scope of this paper and the interested reader is referred to the provided references.

In this study, we employ the SC technique with sparse tensor products based on Clenshaw-Curtis abscissas to compare with the proposed CS approach. For the level parameter of two, one needs 761 LIB simulations in the SC method. Fig. 2(d) compares the validation error in approximating the PC coefficients of the cell capacity obtained by SC and CS methods for the cell discharged at 1C rate. As it can be seen, CS with 761 samples results in the validation errors that are smaller (about one order of magnitude) than those reported by the SC technique. Increasing the level parameter of the SC method to three, in order to increase the accuracy, requires 9976 LIB simulations. A comparison between the level two SC and CS approaches confirms the advantage of our proposed UQ framework, hence, we did not perform level three SC due to the high computational costs. Since we use random samples in CS, unlike in the SC technique, the number of samples are not dictated by the method and one may freely choose a minimum number of additional LIB simulations to achieve the desired accuracy.

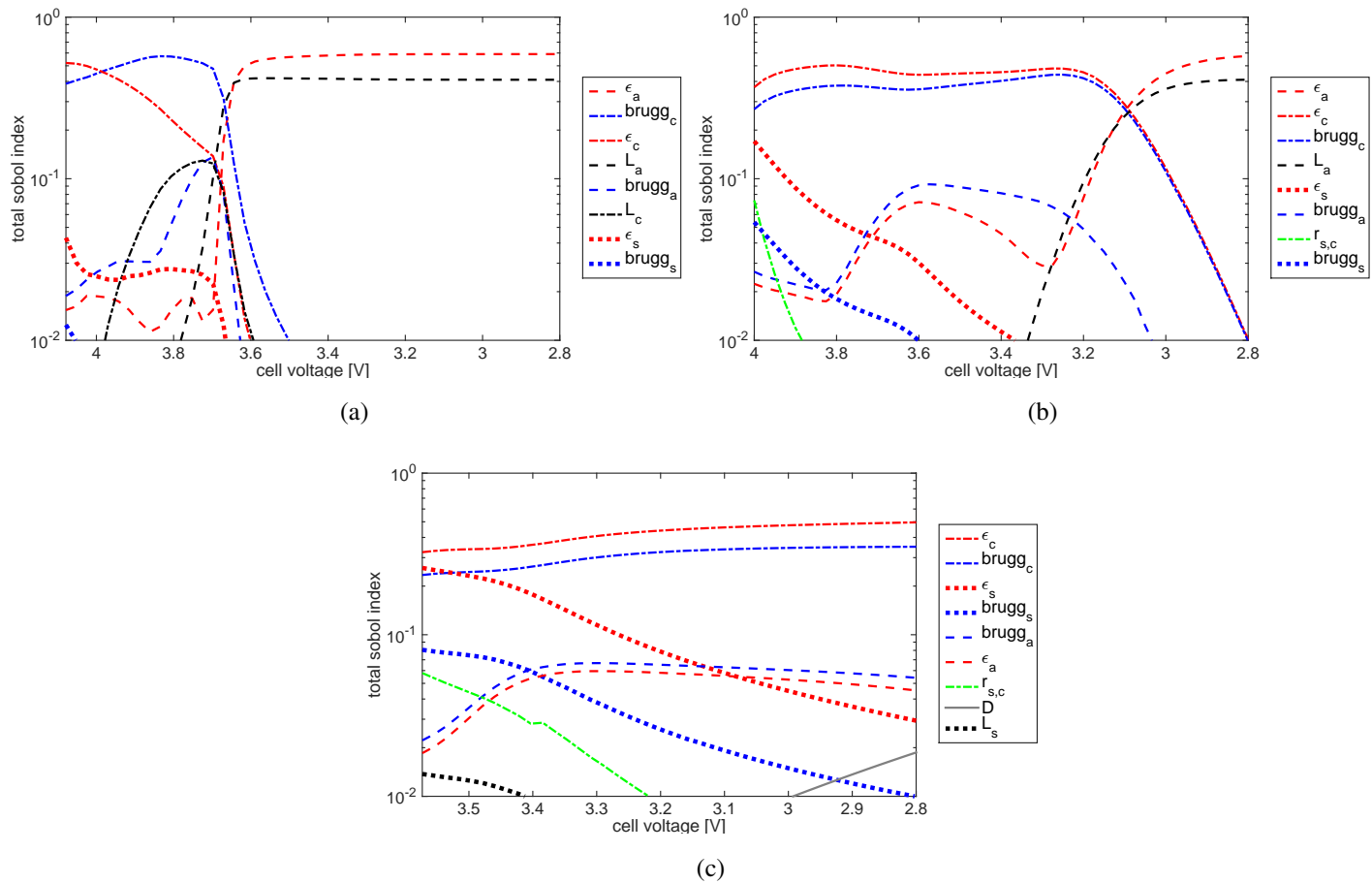


Figure 3: Global sensitivity analysis of the cell capacity for various discharge rates: (a) $I = 0.25C$; (b) $I = 1C$; (c) $I = 4C$.

As discussed in Section 3.2, we compute the total Sobol' indices given in (25) to identify the most important random inputs. We assume that a random input ξ_k with a maximum total Sobol' index S_k^T smaller than 0.01 has no significant effects on the variability of the output QoI and may be treated as a deterministic input. This selection criteria is problem dependent and may be changed depending on the application requirements. Fig. 3 shows the total Sobol' indices associated with the cell capacity over a course of discharge for $I = 0.25C$, $1C$ and $4C$. In this paper, we only present significant Sobol' indices, i.e., those with $\max(S_k^T) > 0.01$, in the global SA plots. Moreover, the legends of the Sobol' index plots are sorted such that the first legend corresponds to the largest S_k^T , while the last legend represents the smallest Sobol' index. The following observations from Fig. 3 are worthwhile highlighting:

- Independent of the discharge rate, porosity ϵ and Bruggeman coefficient brugg in anode, separator, and cathode are among the most important random inputs. In other words, variation in the the cell capacity is highly affected by uncertainty in tortuosity τ .
- For all three discharge rates, Fig. 3 shows that σ_a , σ_c , t_+^0 , $D_{s,a}$, $D_{s,c}$, k_a , k_c , and $r_{s,a}$ are insignificant random inputs and their uncertainties have no important effects on the variability of the cell capacity. Consequently, expensive and accurate quality control measures for these parameters are not required when one aims at reducing the variations in cell capacity.
- As the discharge rate increases, uncertainties in the length of electrodes, i.e., L_a and L_c , become less important, while the effects of variability in the length of separator L_s are more pronounced for $I = 4C$.

- For $I = 4C$, the diffusion coefficient of the liquid phase D is an important random input, while for low to medium rates, its corresponding Sobol' index S_D^T is smaller than 0.01.
- By increasing the discharge rate, the number of important random inputs at the end of discharge increases; two for $I = 0.25C$, four for $I = 1C$, and seven for $I = 4C$. In other words, for high discharge rate LIB applications, accurate quality control measures are needed for a larger number of LIB parameters.
- For low discharge rates, variability in the solid particle size r_s has no significant effects on the variations of the cell capacity.

In general, Fig. 3 suggests that in determining the most significant random inputs on the variations of the LIB capacity, considering the discharge rate is crucial. Again, we emphasize that these observations may change when more accurate LIB models that account for cell degradations and other physical phenomena are employed.

5.1.2. Statistics in normalized time

Since the input samples are different, the battery realizations reach the cut-off potential of 2.8 V at different times. As an example, for 1C rate of discharge, some realizations of the battery reach the cut-off potential before $t = 3200$ s while other realizations need more time, e.g., $t_{max} = 3426$ s. This asynchronous behavior leads to non-smooth dependence of the cell voltage to random inputs and deteriorates the accuracy of PC approximation when the battery approaches the end of discharge.

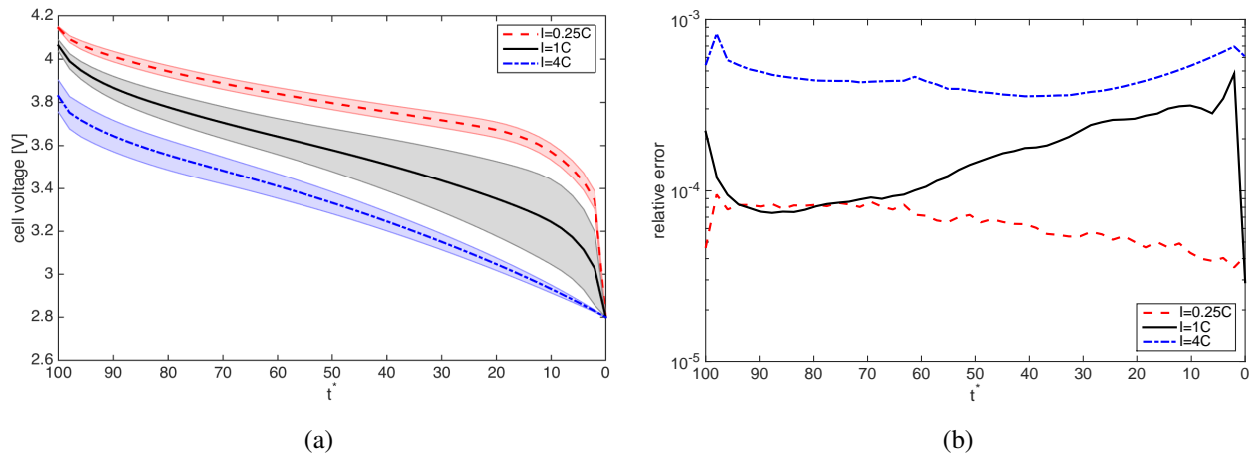


Figure 4: Effects of input uncertainties on the cell voltage for $I = 0.25C$, $1C$ and $4C$ rates of discharge. (a) Mean and standard deviation of the cell voltage. The shaded areas are probability bounds of three standard deviations around the mean; (b) Relative error.

To overcome this issue, we introduce an uncertain time scaling t^* . In order to rescale the deterministic realizations, we assume at $t = 0$, $t^* = 100$, and we set $t^* = 0$ when the battery reaches the cut-off potential of 2.8 V. Hence, at $t^* = 100$ the battery is fully charged and at $t^* = 0$ it is fully discharged. This rescaling approach enables us to maintain the accuracy of approximation over the entire discharge process without increasing the computational cost or complexity of the problem. We note that our definition of t^* involves a constraint on the cell voltage, such that at $t^* = 0$ the cell voltage for all realizations is equal to 2.8 V, which translates to zero variability for the cell voltage at $t^* = 0$. Our t^* definition imposes no constraints on other QoI such as solid and liquid phase concentrations.

5.1.3. Effects of input uncertainties on cell voltage and concentrations

Quantification of the effects of input variations on the cell voltage and concentrations over the charge/discharge processes could provide a better understanding of the cell behavior. In the following, we present the effects of LIB input uncertainties on the stochastic behavior of the cell voltage ϕ_{cell} , liquid phase concentration c , and solid phase concentration at the surface of the solid particle c_s^{surf} as functions of the normalized time t^* . In order to study the variations of c in all three main regions of the LIB, we compute c at three different locations in the cell; middle of anode, separator and cathode. Similarly, c_s^{surf} is computed in the middle of electrodes.

Fig. 4(a) shows the mean and probability bounds of three standard deviations around the mean of cell voltage as the functions of t^* for $I = 0.25\text{C}$, 1C and 4C . Although at $t^* = 100$, larger variabilities in ϕ_{cell} correspond to higher discharge rates, ϕ_{cell} experiences its largest standard deviation at 1C rate of discharge,

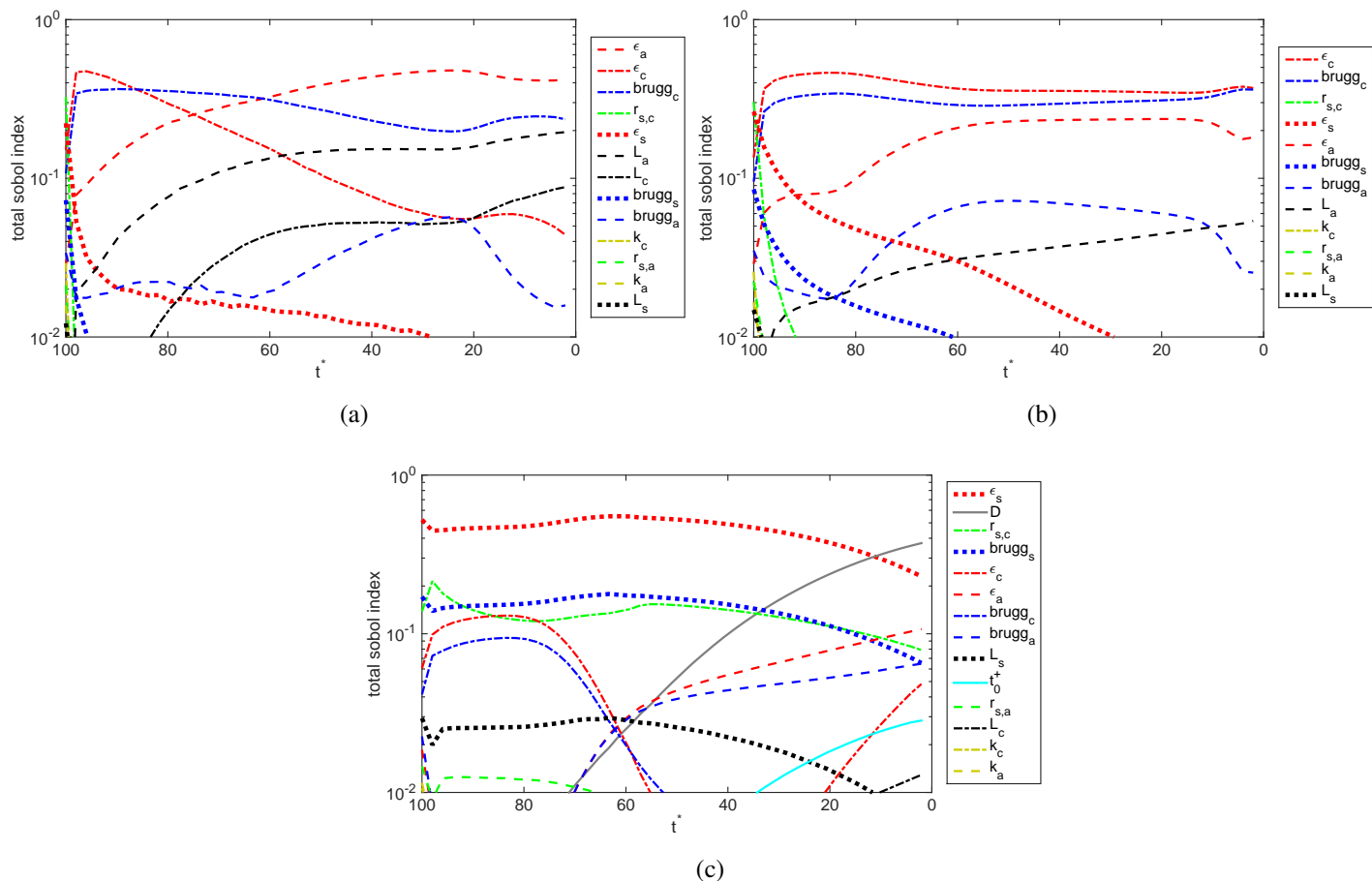


Figure 5: Global sensitivity analysis of the cell voltage for: (a) $I = 0.25C$; (b) $I = 1C$; (c) $I = 4C$.

highlighting again the importance of discharge rate on UQ analysis of the LIBs. The validation error of the PC solution constructed from $N = 1000$ samples is displayed in Fig. 4(b). In fact, $N = 1000$ samples were enough to accurately approximate c and c_s^{surf} as well.

The corresponding total Sobol' indices of the discharge curves in Fig. 4 are presented in Fig. 5, from which we highlight that:

- Similar to the cell capacity, porosity ϵ and Bruggeman coefficient brugg in all three regions are among the most important random inputs which contribute to the variability of the cell voltage for all three discharge rates.

- For all three discharge rates, unlike the cell capacity, uncertainties in k_a , k_c , and $r_{s,a}$ contribute to the cell voltage variations, although, their impacts are limited to the onset of discharge for low to medium discharge rates.
- The uncertainty in σ_a , σ_c , $D_{s,a}$, and $D_{s,c}$ has no significant effects on the variability of the cell voltage.
- As the discharge rate increases, random parameters in separator, i.e., ϵ_s , brugg_s , and L_s , contribute more and more to the cell voltage variations, such that for 4C rate of discharge, ϵ_s becomes the most important random input affecting the cell voltage variability. A similar behavior was observed in Fig. 3.
- For $I = 4C$, variations in the cell voltage are highly affected by the uncertainties in the diffusion coefficient of the liquid phase D . Although, for low to medium discharge rates, D is an insignificant random input, for high discharge rates, its Sobol' index S_D^T grows considerably. Moreover, unlike the cell capacity, Li^+ transference number t_+^0 has a high contribution in the cell voltage variability, when the battery is discharged at 4C rate.
- Similar to the cell capacity, effects of uncertainties in the length of electrodes, L_a and L_c , on the variations of ϕ_{cell} decreases as the rate of discharge increases.

Figs. 6(a)-(c) show the mean values of c and their three standard deviation bounds at three locations for 0.25C, 1C and 4C rates of discharge. As the LIB is discharged at higher rates, larger concentration gradients are developed across the cell to balance the migration of anions [12], as a result of which the liquid

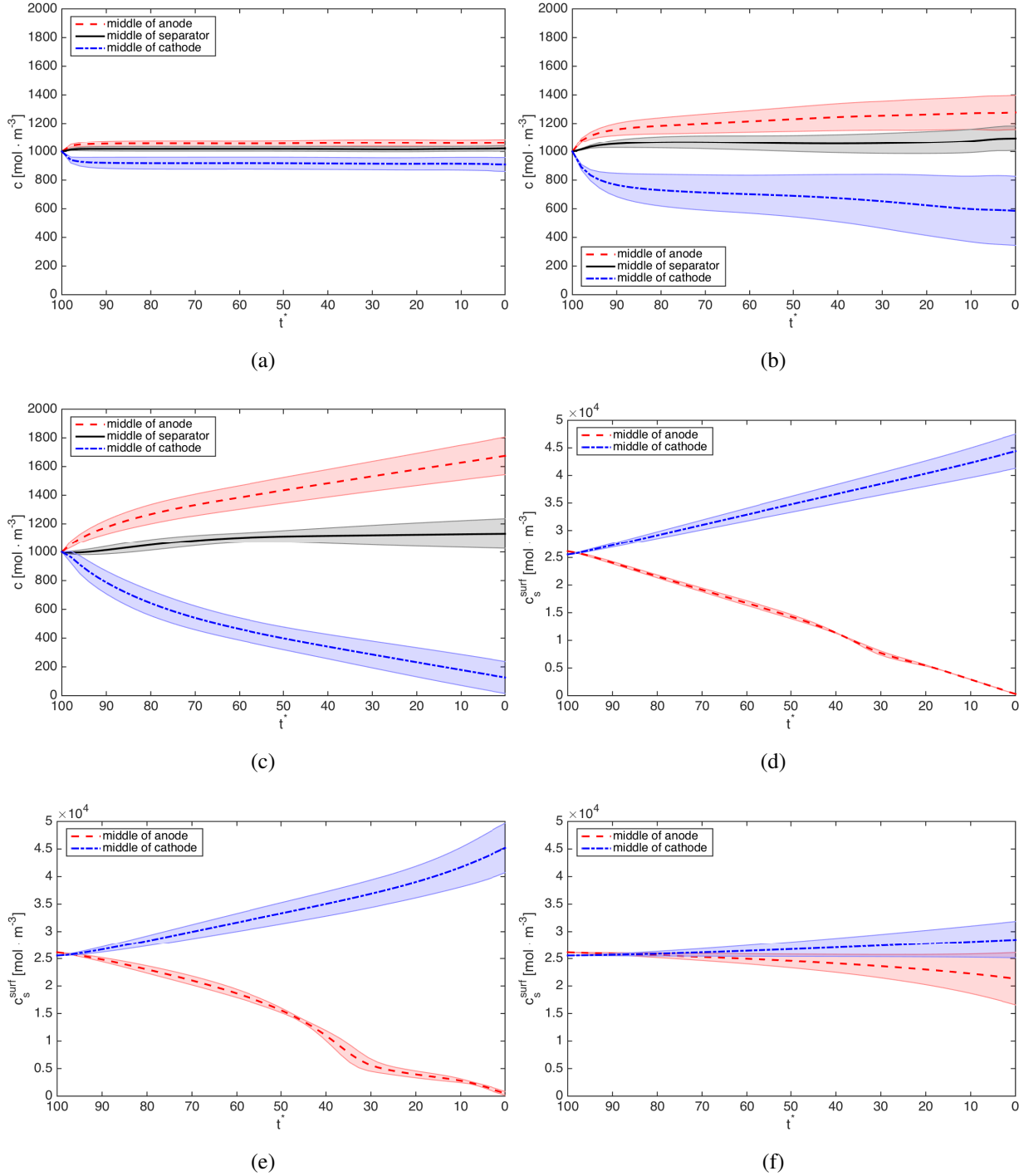


Figure 6: Mean and standard deviation of the liquid phase concentration c in the middle of anode, separator and cathode for: (a) $I = 0.25C$; (b) $I = 1C$; (c) $4C$ rates of discharge. Mean and standard deviation of the solid phase concentration c_s^{surf} in the middle of anode and cathode for: (d) $I = 0.25C$; (e) $I = 1C$; (f) $4C$ rates of discharge. The shaded areas are probability bounds of three standard deviations around the mean.

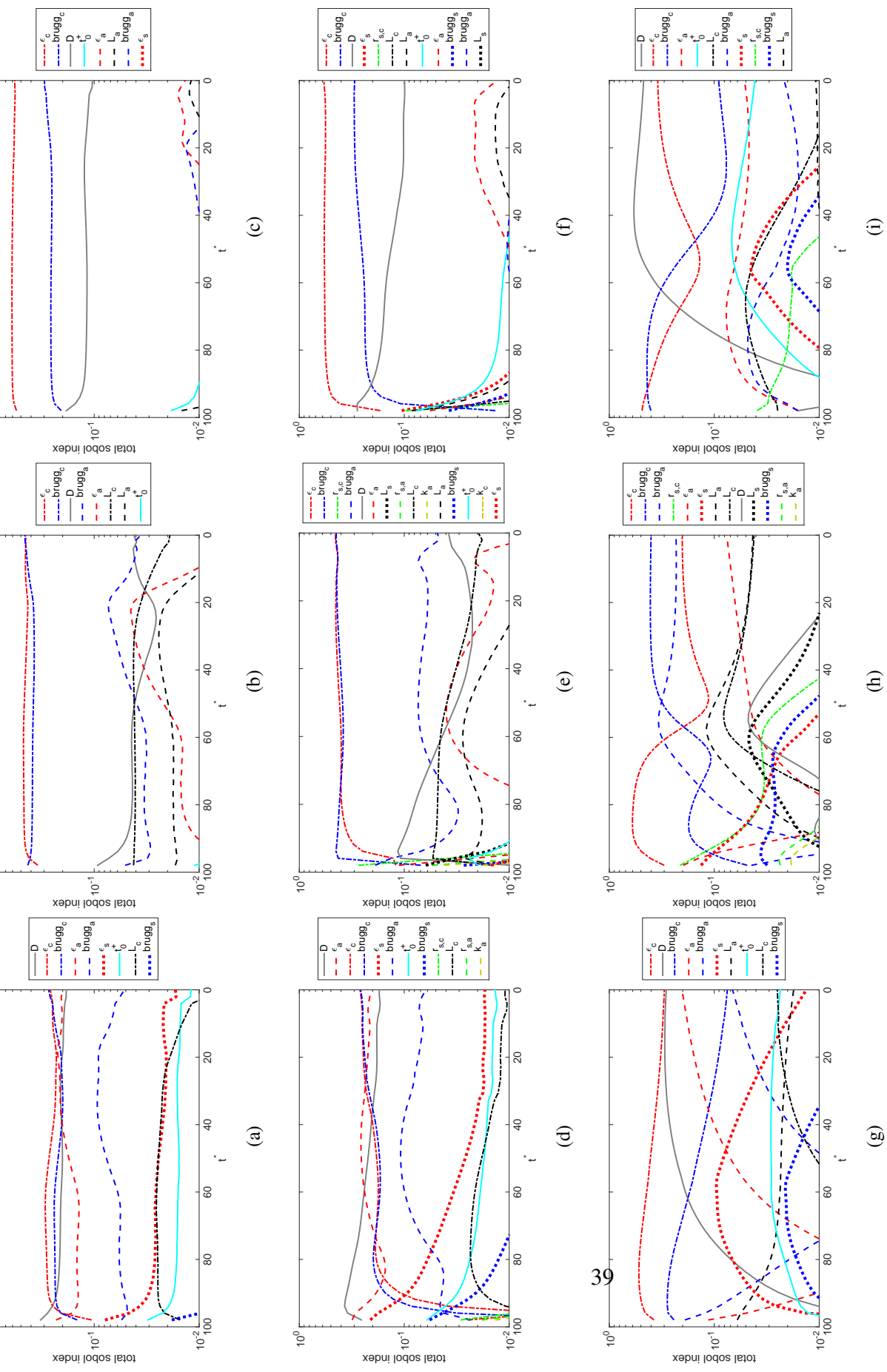


Figure 7: Global sensitivity analysis of the liquid phase concentration for $I = 0.25C$, $1C$ and $4C$ rates of discharge. (a) c in the middle of anode with $I = 0.25C$; (b) c in the middle of separator with $I = 0.25C$; (c) c in the middle of cathode with $I = 0.25C$; (d) c in the middle of anode with $I = 1C$; (e) c in the middle of separator with $I = 1C$; (f) c in the middle of cathode with $I = 1C$; (g) c in the middle of anode with $I = 4C$; (h) c in the middle of separator with $I = 4C$; (i) c in the middle of cathode with $I = 4C$.

concentration in the cathode approaches to zero near the end of discharge for 4C discharge rate (Fig. 6(c)). This may lead to zero concentrations in a region at the back of the cathode electrode, which means the active materials may not be utilized further. This limits the capability of the LIB to be discharged at higher rates. On the other hand, high concentrations in the anode electrode may be problematic when the lithium salt/solvent system used has a solubility limit. For example, such a limit is 2100 mol/m^3 for Lithium Perchlorate in Propylene Carbonate at room temperature [12]. Consequently, analysis of the variability of liquid phase concentration near the end of discharge may provide a more accurate understanding of the rate limiting mechanisms associated with diffusion of lithium ions. As can be observed from this figure, our definition of t^* does not impose any constraints on c ; hence, unlike the cell voltage, variability of c is not equal to zero at $t^* = 0$.

As mentioned in Section 4, it has been shown that σ and D_s depend on the solid phase concentration. Taking into account the variability in the solid phase concentration due to input variations may help to assess such dependencies more accurately. A similar analysis is performed for the solid phase concentration at the surface of the solid particle c_s^{surf} . The mean values of c_s^{surf} bounded by three standard deviations in the middle of electrodes for $I = 0.25\text{C}$, 1C and 4C rates of discharge are also presented in Figs. 6(d)-(f). It can be observed that the variability of c_s^{surf} in the middle of the anode does not grow significantly as the battery is discharged at low and medium rates, while for the high discharge rate, standard deviation of c_s^{surf} in both electrodes is increased monotonically over the course of discharge.

Fig. 7 shows the corresponding total Sobol' indices of c in three regions for $I = 0.25\text{C}$, 1C and 4C rates of discharge. We observe that for low to medium dis-

charge rates, the influential random inputs on the variability of c vary considerably from one region to another. As an instance, for $I = 0.25C$, variations in c in the middle of cathode are mainly affected by uncertainty in ϵ_c , brugg_c , and D , while in the anode, these variations are affected by the uncertainty in D , ϵ_c , brugg_c , ϵ_a , brugg_a , ϵ_s , t_+^0 , L_c , and brugg_s . In other words, for low discharge rates, variability of c in the anode is affected by the random inputs associated with the other two regions, i.e., separator and cathode, while this is not true for the variation of c in the cathode. Additionally, we note that:

- Similar to the cell capacity and voltage, uncertainties in σ_a , σ_c , $D_{s,a}$, and $D_{s,c}$ have no significant effects on the variability of c . Moreover, although reaction rate constants k_a and k_c appear in Figs. 7(d), (e), and (h), their impact on the variability of c is small.
- Despite the discharge rate in all three regions, uncertainty in D and t_+^0 has more pronounced effects on the variation of c in both electrodes in comparison to separator.
- S_D^T is increased in the electrodes and decreased in the separator as the LIB is discharged at higher rates.
- Unlike the cell capacity and voltage, the effect of uncertainties in the length of the electrodes L_a and L_c on the variations of c increases as the rate of discharge increases.

A global SA of c_s^{surf} in both electrodes is also presented in Fig. 8. We see that uncertainty in the solid phase diffusion coefficient D_s has no significant effects on

the variability of cell capacity, voltage and liquid phase concentration. Surprisingly, D_s may be labeled as an insignificant random input even on the variations of c_s^{surf} in both electrodes for all three discharge rates. Moreover, the uncertainty in σ_a and σ_c also has no impacts on the variability of c_s^{surf} independent of the discharge rate. As the LIB experiences higher discharge rates, the total Sobol' index of $r_{s,a}$ decreases, while for $r_{s,c}$, an increase in the total Sobol' index is observed.

In summary, we see that in our stochastic LIB example, the uncertainty in σ and D_s has no significant effects on the variability of the cell capacity, voltage and concentrations, hence, may be treated as deterministic inputs. Because of this, tight quality control measures are not needed for these parameters. On the other hand, ϵ and brugg are the most important random inputs independent of the discharge rate, and require tight quality control measures to reduce the LIB cell-to-cell variations. Moreover, we observe that the relative contribution of uncertainty in the model parameters in the overall performance variability is highly affected by the battery discharge rate.

We emphasize that the results presented in this section apply only to the $\text{LiC}_6/\text{LiCoO}_2$ cell we consider in this study subjected to the input variabilities presented in Table 3. Any changes in these uncertainties or cell chemistry/configuration may result in different observations. This is also the case if a more accurate LIB model, which accounts for additional physical and chemical phenomena, is employed.

6. Conclusion

A sampling-based UQ approach was introduced to study the effects of input uncertainties on the performance of the LIBs. The proposed UQ approach is based on polynomial chaos expansion framework and hinges on a sparse approx-

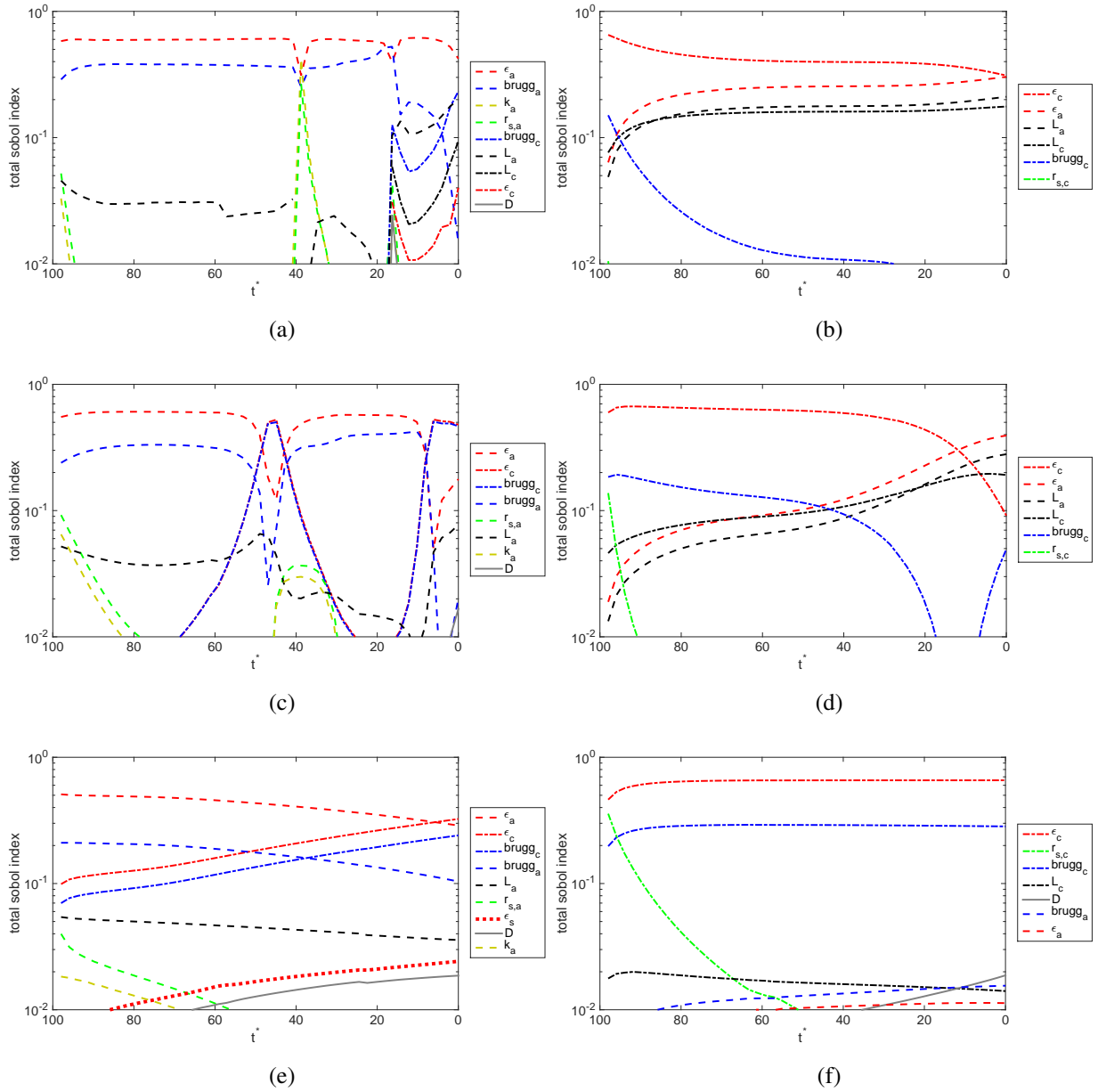


Figure 8: Sensitivity analysis of the solid phase concentration for $I = 0.25C$, $1C$ and $4C$ rates of discharge. (a) c_s^{surf} in the middle of anode with $I = 0.25C$; (b) c_s^{surf} in the middle of cathode with $I = 0.25C$; (c) c_s^{surf} in the middle of anode with $I = 1C$; (d) c_s^{surf} in the middle of cathode with $I = 1C$; (e) c_s^{surf} in the middle of anode with $I = 4C$; (f) c_s^{surf} in the middle of cathode with $I = 4C$.

imation technique to achieve an accurate estimation of solution statistics with a small number of LIB simulations. Additionally, the proposed method enables one to identify the most important random inputs for any QoI such as capacity, voltage, and concentrations by performing a global sensitivity analysis via computing the total Sobol' indices. Such an analysis is helpful in designing more efficient and targeted quality control measures, from material selection to cell assembly, and reducing the manufacturing cost of the LIBs.

Performance of the proposed UQ approach was explored through its application to an $\text{LiC}_6/\text{LiCoO}_2$ LIB discharged at three different rates. It was shown that the proposed UQ method can accurately compute the variability in the output QoIs such as the cell capacity, voltage, and concentrations with a small number of battery simulations, 1000 in this example. The global sensitivity analysis results corresponding to these QoIs showed that the identification of the most important uncertain inputs is highly affected by the battery discharge rate. For all three discharge rates, we found that the porosity and Bruggeman coefficient are among the most significant uncertain parameters in the performance variability of the examined LIB.

We acknowledge that the LIB model we considered in this study suffers from many unmodeled phenomena such as side reactions, stresses associated with volume changes, cell degradation, and temperature dependence, which may affect the stochastic behavior of the cell. Since the proposed stochastic LIB model is based on sampling, in order to include these phenomena in the model, more accurate LIB models can be incorporated without changing the overall UQ framework. This may, however, increase the number of required battery simulations and, hence, the overall computational cost. Additionally, the accuracy of the uncertainty models

we adopted for the LIB input parameters is limited by the available experimental data. For some of these inputs, data are highly sparse or non-existent. We, therefore, resorted to assumptions in describing the uncertainty. When data becomes available, these uncertainty models may be improved accordingly.

The proposed UQ framework in this study was developed for forward propagation of the uncertainties in the LIB simulations. Interesting future research directions include using this forward UQ framework along with actual experimental data to infer battery model parameters as well as quantitative validation of the model itself.

Acknowledgements

MH is immensely grateful to Dr. Jan Reimers for his fruitful comments on coding the decoupled formulation of LIBs and also Dr. Sehee Lee for his comments on the experimental techniques.

MH and KM's work was supported by the National Science Foundation grant CMMI-1201207. This material is based upon work of AD supported by the U.S. Department of Energy Office of Science, Office of Advanced Scientific Computing Research, under Award Number de-sc0006402 and NSF grant CMMI-1454601.

This work utilized the Janus supercomputer, which is supported by the National Science Foundation (award number CNS-0821794) and the University of Colorado Boulder. The Janus supercomputer is a joint effort of the University of Colorado Boulder, the University of Colorado Denver and the National Center for Atmospheric Research.

Appendix A. A decoupled formulation for LIBs

The decoupling procedure starts with combining the potential equations for the solid phase (9), liquid phase (8) and the Butler-Volmer (BV) equation (10) in order to first reduce the number of equations to be solved. This is motivated by the fact that in each electrode, there are only three tightly coupled quantities, i.e., c , c_s and the over-potential $\eta = \phi_s - \phi_e - V$, which need to be solved simultaneously [51]. Consequently, the following non-linear equation for the over-potential η can be obtained

$$\begin{aligned} \nabla(\sigma^h \nabla \eta) &= ai_{ex} \left[\exp\left(\frac{0.5F\eta}{RT}\right) - \exp\left(-\frac{0.5F\eta}{RT}\right) \right] \\ &\quad - \nabla \left[\frac{I}{\sigma^{\text{eff}}} + \frac{\kappa_D^{\text{eff}}}{\kappa^{\text{eff}}} \nabla \ln c(\eta) + \nabla V(\eta) \right], \end{aligned} \quad (\text{A.1})$$

subjected to the boundary conditions

$$\nabla \eta|_{x=0,L} = - \left[\frac{I}{\sigma^{\text{eff}}} + \nabla V(\eta) \right]_{x=0,L}, \quad (\text{A.2})$$

$$\nabla \eta|_{x=L_a, L_a+L_s} = \left[\frac{I}{\kappa^{\text{eff}}} - \frac{\kappa_D^{\text{eff}}}{\kappa^{\text{eff}}} \nabla \ln c(\eta) - \nabla V(\eta) \right]_{x=L_a, L_a+L_s}. \quad (\text{A.3})$$

Here, σ^h is the harmonic mean conductivity defined by $\frac{1}{\sigma^h} = \frac{1}{\sigma^{\text{eff}}} + \frac{1}{\kappa^{\text{eff}}}$. So far, instead of solving the coupled system of equations in Table 1, one needs to solve a system of equations including Eqs. (6), (7) and (A.1) simultaneously. We note that all of the nonlinearities are isolated in Eq. (A.1) for the over-potential.

The next step of deriving the reformulation is decoupling these three equations via the concept of particular and homogeneous solutions to ODEs. Application of the implicit finite time differencing to the solid phase diffusion equation (7) results in the following non-homogeneous ODE with non-homogeneous BCs

$$c_s(r, t + \Delta t) - \frac{\Delta t}{r^2} \frac{\partial}{\partial r} \left(D_s r^2 \frac{\partial}{\partial r} c_s(r, t + \Delta t) \right) = c_s(r, t), \quad (\text{A.4})$$

$$\nabla c_s|_{r=0} = 0, \quad \nabla c_s|_{r=r_s} = -\frac{j_{vol}}{aFD_s}. \quad (\text{A.5})$$

One may write the general solution to Eq. (A.4) as

$$c_s(r, t + \Delta t) = c_s^o(r, t + \Delta t) + \frac{j_{vol}}{aF} c_s^j(r, t + \Delta t), \quad (\text{A.6})$$

where c_s^o is the solution to the following non-homogeneous ODE with homogeneous BCs

$$c_s^o(r, t + \Delta t) - \frac{\Delta t}{r^2} \frac{\partial}{\partial r} \left(D_s r^2 \frac{\partial}{\partial r} c_s^o(r, t + \Delta t) \right) = c_s(r, t), \quad (\text{A.7})$$

$$\nabla c_s^o|_{r=0} = 0, \quad \nabla c_s^o|_{r=r_s} = 0, \quad (\text{A.8})$$

and c_s^j is the solution to the following the homogeneous ODE with non-homogeneous BCs

$$c_s^j(r, t + \Delta t) - \frac{\Delta t}{r^2} \frac{\partial}{\partial r} \left(D_s r^2 \frac{\partial}{\partial r} c_s^j(r, t + \Delta t) \right) = 0, \quad (\text{A.9})$$

$$\nabla c_s^j|_{r=0} = 0, \quad \nabla c_s^j|_{r=r_s} = -\frac{1}{D_s}. \quad (\text{A.10})$$

A similar approach may be employed for decoupling the solution of the electrolyte phase diffusion equation (6) from the over-potential solution η and the volumetric pore wall flux j_{vol} . The only difference here is that j_{vol} in Eq. (6) is a position dependent source term while in Eq. (7) it appears on the boundary conditions. Consequently, the general solution to the discretized version of Eq. (6) in the time domain can be obtained via

$$c(x, t + \Delta t) = c^o(x, t + \Delta t) + \frac{1 - t_+}{F} \int j_{vol}(x_0) c^j(x, x_0, t + \Delta t) dx_0. \quad (\text{A.11})$$

Here in Eq. (A.11), c^o and c^j are the solutions to the following ODEs both subjected to zero flux boundary conditions

$$\frac{\epsilon[c^o(x, t + \Delta t) - c(x, t)]}{\Delta t} = \nabla[\epsilon D^{\text{eff}} \nabla c^o(x, t + \Delta t)], \quad (\text{A.12})$$

$$\frac{\epsilon c^j(x, x_0, t + \Delta t)}{\Delta t} = \nabla[\epsilon D^{\text{eff}} \nabla c^j(x, x_0, t + \Delta t)] + \delta(x - x_0), \quad (\text{A.13})$$

with $\delta(x - x_0)$ being the Dirac delta function.

At this point, solutions to the solid and electrolyte phase diffusion equations are decoupled from the over-potential and pore wall flux since in solving Eqs. (A.7), (A.9), (A.12) and (A.13), η and j_{vol} are not needed. Moreover, for the cases when D_s , D^{eff} and ϵ are constant, analytic solutions are available for Eqs. (A.9) and (A.13) [51]. c_s^j and c^j can also be used to obtain a linearized form for the terms including $V(\eta)$ and $\ln c(\eta)$ on the RHS of Eq. (A.1), respectively. In conclusion, one needs to solve the decoupled Eqs. (A.7), (A.9), (A.12), (A.13), and (A.1) instead of solving the coupled system of non-linear equations in Table 1 for LIB modeling. In addition, if a constant time step is used, Eqs. (A.9) and (A.13) need to be solved once at the beginning of the simulation. The only major approximation in deriving this decoupled formulation is the finite time differencing which is inevitable in numerical simulations. An extended version of this decoupled formulation, which includes SEI resistance and double layer capacitive effects coupled with a thermal model, is given in [96, 97]. Interested reader is

referred to [51] for more details on linearizing the over-potential equation (A.1), grid generation and the time evolution strategy.

References

References

- [1] S. Golmon, K. Maute, and M.L. Dunn. Numerical modeling of electrochemical-mechanical interactions in Lithium polymer batteries. *Computers and Structures*, 87:1567–1579, 2009.
- [2] Marc Doyle and Yuris Fuentes. Computer simulations of a Lithium-ion polymer battery and implications for higher capacity next-generation battery designs. *Journal of The Electrochemical Society*, 150:A706–A713, 2003.
- [3] R.A Marsh, S Vukson, S Surampudi, B.V Ratnakumar, M.C Smart, M Manzo, and P.J Dalton. Li ion batteries for aerospace applications. *Journal of Power Sources*, 97–98:25–27, 2001.
- [4] Vinodkumar Etacheri, Rotem Marom, Ran Elazari, Gregory Salitra, and Doron Aurbach. Challenges in the development of advanced Li-ion batteries: a review. *Energy Environ. Sci.*, 4:3243, 2011.
- [5] Karen E. Thomas, John Newman, and Robert M. Darling. Mathematical modeling of Lithium batteries. In Walter A. Schalkwijk and Bruno Scrosati, editors, *Advances in Lithium-Ion Batteries*, pages 345–392. Springer USA, 2002.
- [6] M. Doyle, T.F. Fuller, and J. Newman. Modeling of galvanostatic charge and discharge of the Lithium/polymer/insertion cell. *Journal of the Electrochemical Society*, 140(6):1526–1533, 1993.

- [7] Kandler A. Smith, Christopher D. Rahn, and Chao-Yang Wang. Model order reduction of 1d diffusion systems via residue grouping. *J. Dyn. Sys., Meas., Control*, 130:011012, 2008.
- [8] Long Cai and Ralph E. White. Reduction of model order based on proper orthogonal decomposition for Lithium-ion battery simulations. *J. Electrochem. Soc.*, 156:A154–A161, 2009.
- [9] Venkat R. Subramanian, Vijayasekaran Boovaragavan, Venkatasailanathan Ramadesigan, and Mounika Arabandi. Mathematical model reformulation for Lithium-ion battery simulations: Galvanostatic boundary conditions. *Journal of The Electrochemical Society*, 156:A260–A271, 2009.
- [10] Joel C. Forman, Saeid Bashash, Jeffrey L. Stein, and Hosam K. Fathy. Reduction of an electrochemistry-based Li-ion battery model via quasi-linearization and pade approximation. *J. Electrochem. Soc.*, 158:A93–A101, 2011.
- [11] Wenbo Du, Nansi Xue, Wei Shyy, and Joaquim R. R. A. Martins. A surrogate-based multi-scale model for mass transport and electrochemical kinetics in Lithium-ion battery electrodes. *J. Electrochem. Soc.*, 161:E3086–E3096, 2014.
- [12] Thomas F. Fuller, Marc Doyle, and John Newman. Simulation and optimization of the dual Lithium ion insertion cell. *Journal of The Electrochemical Society*, 141:1–10, 1994.
- [13] Stephanie Golmon, Kurt Maute, and Martin L. Dunn. A pomegranate-inspired nanoscale design for large-volume-change Lithium battery anodes.

International Journal for Numerical Methods in Engineering, 92:475–494, 2012.

- [14] Nansi Xue, Wenbo Du, Amit Gupta, Wei Shyy, Ann Marie Sastry, and Joaquim R. R. A. Martins. Optimization of a single Lithium-ion battery cell with a gradient-based algorithm batteries and energy storage. *J. Electrochem. Soc.*, 160:A1071–A1078, 2013.
- [15] Jiajun Chen. Recent progress in advanced materials for Lithium ion batteries. *Materials*, 6:156–183, 2013.
- [16] Hongchang Pang, Peng Cheng, Hongbin Yang, Jinlin Lu, Chun Xian Guo, Guiling Ning, and Chang Ming Li. Template-free bottom-up synthesis of yolk-shell vanadium oxide as high performance cathode for Lithium ion batteries. *Chem. Commun.*, 49:1536–1538, 2013.
- [17] Vanchiappan Aravindan, Joe Gnanaraj, Yun-Sung Lee, and Srinivasan Madhavi. LiMnPO_4 - a next generation cathode material for Lithium-ion batteries. *J. Mater. Chem. A*, 1:3518–3539, 2013.
- [18] John Newman and William Tiedemann. Porous-electrode theory with battery applications. *AIChE Journal*, 21(1):25–41, 1975.
- [19] Marc Doyle, John Newman, Antoni S. Gozdz, Caroline N. Schmutz, and JeanMarie Tarascon. Comparison of modeling predictions with experimental data from plastic Lithium ion cells. *J. Electrochem. Soc.*, 143:1890–1903, 1996.
- [20] Shriram Santhanagopalan and Ralph E. White. Modeling parametric uncertainty using polynomial chaos theory. *ECS Trans.*, 3:243–256, 2007.

- [21] Malvern Instruments Ltd. Mastersizer 2000 user manual. <http://www.malvern.com>, 2007. Accessed: 2014-07-29.
- [22] R. Darling and J. Newman. Modeling a porous intercalation electrode with two characteristic particle sizes. *J. Electrochem. Soc.*, 144:4201–4208, 1997.
- [23] G. S. Nagarajan, J. W. Van Zee, and R. M. Spotnitz. A mathematical model for intercalation electrode behavior: I. effect of particle-size distribution on discharge capacity. *J. Electrochem. Soc.*, 145:771–779, 1998.
- [24] C. Y. Wang and V. Srinivasan. Computational battery dynamics (cbd)electrochemical/thermal coupled modeling and multi-scale modeling. *Journal of Power Sources*, 110:364–376, 2002.
- [25] D. E. Stephenson, E. M. Hartman, J. N. Harb, and D. R. Wheeler. Modeling of particle-particle interactions in porous cathodes for Lithium-ion batteries. *J. Electrochem. Soc.*, 154:A1146–A1155, 2007.
- [26] Sankaran Mahadevan. Uncertainty quantification for decision-making in engineered systems. In Subrata Chakraborty and Gautam Bhattacharya, editors, *Proceedings of the International Symposium on Engineering under Uncertainty: Safety Assessment and Management (ISEUSAM - 2012)*, pages 97–117. Springer India, 2013.
- [27] Eric Bickel and Reidar Bratvold. From uncertainty quantification to decision making in the oil and gas industry. *Energy, Exploration & Exploitation*, 26(5):311–325, 2008.
- [28] Shankar Sankararaman and Kai Goebel. Uncertainty quantification in remaining useful life of aerospace components using state space models and

- inverse form. *54th AIAA/ASME/ASCE/AHS/ASC Structures, Structural Dynamics, and Materials Conference*, 2013.
- [29] D. Xiu. *Numerical Methods for Stochastic Computations: A Spectral Method Approach*. Princeton University Press, 2010.
- [30] O.P. Le Maitre and O. Knio. A stochastic particle-mesh scheme for uncertainty propagation in vortical flows. *J. Comput. Phys.*, 226:645771, 2007.
- [31] John Milburn Mcfarland. *Uncertainty Analysis for Computer Simulations Through Validation and Calibration*. PhD thesis, Nashville, TN, USA, 2008. AAI3378200.
- [32] Dimitris Bertsimas and Aurlie Thiele. *Robust and Data-Driven Optimization: Modern Decision Making Under Uncertainty*, chapter 5, pages 95–122. 2014.
- [33] Rgis Duvigneau, Massimiliano Martinelli, and Praveen Chandrashekarappa. *Uncertainty Quantification for Robust Design*, pages 405–424. John Wiley & Sons, Inc., 2013.
- [34] Andrzej Banaszuk, Vladimir A. Fonoberov, Thomas A. Frewen, Marin Kobilarov, George Mathew, Igor Mezic, Alessandro Pinto, Tuhin Sahai, Harshad Sane, Alberto Speranzon, and Amit Surana. Scalable approach to uncertainty quantification and robust design of interconnected dynamical systems. *Annual Reviews in Control*, 35(1):77 – 98, 2011.
- [35] R. Ghanem and P. Spanos. *Stochastic Finite Elements: A Spectral Approach*. Springer Verlag, 1991.

- [36] N. Wiener. The homogeneous chaos. *Amer. J. Math*, 60:897–936, 1938.
- [37] R.H. Cameron and W.T. Martin. The orthogonal development of nonlinear functionals in series of Fourier-Hermite functionals. *Ann. Math.*, 48:385–392, 1947.
- [38] O.P. Le Maitre and O. Knio. *Spectral Methods for Uncertainty Quantification with Applications to Computational Fluid Dynamics*. Springer, 2010.
- [39] S. Hosder, R.W. Walters, and R. Perez. A non-intrusive polynomial chaos method for uncertainty propagation in CFD simulations. In *44th AIAA aerospace sciences meeting and exhibit, AIAA-2006-891*, Reno (NV), 2006.
- [40] A. Doostan and H. Owhadi. A non-adapted sparse approximation of PDEs with stochastic inputs. *Journal of Computational Physics*, 230:3015–3034, 2011.
- [41] Jerrad Hampton and Alireza Doostan. Compressive sampling of polynomial chaos expansions: Convergence analysis and sampling strategies. *Journal of Computational Physics*, 280(0):363 – 386, 2015.
- [42] Jerrad Hampton and Alireza Doostan. Coherence motivated sampling and convergence analysis of least squares polynomial chaos regression. *Computer Methods in Applied Mechanics and Engineering*, 290(0):73 – 97, 2015.
- [43] P. G. Constantine, M. Eldred, and E. Phipps. Sparse pseudospectral approximation method. *Computer Methods in Applied Mechanics and Engineering*, 229:1–12, 2012.

- [44] Wenbo Dua, Amit Gupta, Xiangchun Zhang, Ann Marie Sastry, and Wei Shyy. Effect of cycling rate, particle size and transport properties on Lithium-ion cathode performance. *International Journal of Heat and Mass Transfer*, 53:3552–3561, 2010.
- [45] Shriram Santhanagopalan and Ralph E. White. Quantifying cell-to-cell variations in Lithium ion batteries. *International Journal of Electrochemistry*, 2012:Article ID 395838, 2012.
- [46] Godfrey Sikha and Ralph E. White. Analytical expression for the impedance response for a lithium-ion cell. *Journal of The Electrochemical Society*, 155(12):A893–A902, 2008.
- [47] Venkatasailanathan Ramadesigan, Kejia Chen, Nancy A. Burns, Vijayasekaran Boovaragavan, Richard D. Braatz, and Venkat R. Subramanian. Parameter estimation and capacity fade analysis of Lithium-ion batteries using reformulated models. *Journal of The Electrochemical Society*, 158:A1048–A1054, 2011.
- [48] Donghwa Shin, M. Poncino, E. Macii, and Naehyuck Chang. A statistical model of cell-to-cell variation in li-ion batteries for system-level design. In *Low Power Electronics and Design (ISLPED), 2013 IEEE International Symposium on*, pages 94–99, Sept 2013.
- [49] P. Popov, Y. Vutov, S. Margenov, and O. Iliev. Finite volume discretization of equations describing nonlinear diffusion in Li-ion batteries. In Ivan Dimov, Stefka Dimova, and Natalia Kolkovska, editors, *Numerical Methods*

- and Applications*, volume 6046 of *Lecture Notes in Computer Science*, pages 338–346. Springer Berlin Heidelberg, 2011.
- [50] C. Y. Wang, W. B. Gu, and B. Y. Liaw. Micromacroscopic coupled modeling of batteries and fuel cells: I. model development. *J. Electrochem. Soc.*, 145:3407–3417, 1998.
- [51] Jan N. Reimers. Algorithmic improvements and PDE decoupling, for the simulation of porous electrode cells. *J. Electrochem. Soc.*, 160:A811–A818, 2013.
- [52] D. Xiu and G.M. Karniadakis. The Wiener-Askey polynomial chaos for stochastic differential equations. *SIAM Journal on Scientific Computing*, 24(2):619–644, 2002.
- [53] M. S. Eldred. Recent advances in non-intrusive polynomial chaos and stochastic collocation methods for uncertainty analysis and design. In *50th AIAA/ASME/ASCE/AHS/ASC Structures, Structural Dynamics, and Materials Conference*, Palm Springs, CA, 2009.
- [54] Bruno Sudret. Global sensitivity analysis using polynomial chaos expansions. *Reliability Engineering and System Safety*, 93(7):964 – 979, 2008.
- [55] Ji Peng, Jerrad Hampton, and Alireza Doostan. A weighted l_1 -minimization approach for sparse polynomial chaos expansions. *Journal of Computational Physics*, 267(0):92 – 111, 2014.
- [56] Daniele Schiavazzi, Alireza Doostan, and Gianluca Iaccarino. Sparse multiresolution regression for uncertainty propagation. *International Journal for Uncertainty Quantification*, 4(4):303–331, 2014.

- [57] Liang Yan, Ling Guo, and Dongbin Xiu. Stochastic collocation algorithms using l_1 -minimization. *International Journal for Uncertainty Quantification*, 2(3):279–293, 2012.
- [58] Brandon A. Jones, Nathan Parrish, and Alireza Doostan. Postmaneuver collision probability estimation using sparse polynomial chaos expansions. *Journal of Guidance, Control, and Dynamics*, pages 1–13, 2015.
- [59] Xiu Yang and George Em Karniadakis. Reweighted l_1 minimization method for stochastic elliptic differential equations. *Journal of Computational Physics*, 248(0):87 – 108, 2013.
- [60] D.L. Donoho. Compressed sensing. *IEEE Transactions on information theory*, 52(4):1289–1306, 2006.
- [61] A.M. Bruckstein, D.L. Donoho, and M. Elad. From sparse solutions of systems of equations to sparse modeling of signals and images. *SIAM Review*, 51(1):34–81, 2009.
- [62] E.J. Candes and T. Tao. Near optimal signal recovery from random projections: Universal encoding strategies? *IEEE Transactions on information theory*, 52(12):5406–5425, 2006.
- [63] E. van den Berg and M. P. Friedlander. Probing the Pareto frontier for basis pursuit solutions. *SIAM Journal on Scientific Computing*, 31(2):890–912, 2008.
- [64] E. van den Berg and M. P. Friedlander. SPGL1: A solver for large-scale sparse reconstruction, June 2007. Available from <http://www.cs.ubc.ca/labs/scl/spgl1>.

- [65] I.M. Sobol'. Global sensitivity indices for nonlinear mathematical models and their monte carlo estimates. *Mathematics and Computers in Simulation*, 55(13):271 – 280, 2001.
- [66] P.R. Shearing, L.E. Howard, P.S. Jorgensen, N.P. Brandon, and S.J. Harris. Characterization of the 3-dimensional microstructure of a graphite negative electrode from a Li-ion battery. *Electrochemistry Communications*, 12:374–377, 2010.
- [67] Tyler DuBeshter, Puneet K. Sinha, Alex Sakars, Gerald W. Fly, , and Jacob Jorne. Measurement of tortuosity and porosity of porous battery electrodes. *J. Electrochem. Soc.*, 161:A599–A605, 2014.
- [68] Sheng Shui Zhang. A review on the separators of liquid electrolyte Li-ion batteries. *Journal of Power Source*, 164:351–364, 2007.
- [69] Ding-Wen Chung, Paul R. Shearing, Nigel P. Brandon, Stephen J. Harris, and R. Edwin Garcia. Particle size polydispersity in Li-ion batteries. *J. Electrochem. Soc.*, 161:A422–A430, 2014.
- [70] Chuen-Shii Chou, Ching-Hua Tsou, and Chin-I Wang. Preparation of graphite/nano-powder composite particles and applicability as carbon anode material in a Lithium ion battery. *Advanced Powder Technology*, 19:383–396, 2008.
- [71] John R. Izzo Jr., Abhijit Joshi, Kyle Grew, Wilson Chiu, Andrei Tkachuk, Siew Wang, and Wenbing Yun. Nondestructive reconstruction and analysis of solid oxide fuel cell anodes using x-ray computed tomography at sub-50 nm resolution. *J. Electrochem. Soc.*, 155:B504–B508, 2008.

- [72] P.R. Shearing, J. Golbert, R.J. Chater, and N.P. Brandon. 3D reconstruction of SOFC anodes using a focused ion beam lift-out technique. *Chemical Engineering Science*, 64:3928–3933, 2009.
- [73] Indrajeet V. Thorat, David E. Stephenson, Nathan A. Zachariasa, Karim Zaghbib, John N. Harba, and Dean R. Wheeler. Quantifying tortuosity in porous Li-ion battery materials. *Journal of Power Sources*, 188:592–600, 2009.
- [74] M. Ebner, Ding-Wen Chung, R. E. Garcia, and V. Wood. Tortuosity anisotropy in Lithium-ion battery electrodes. *Adv. Energy Mater.*, 4:1301278, 2014.
- [75] S. Zugmann, M. Fleischmann, M. Amereller, R.M. Gschwind, H.D. Wiemhofer, and H.J. Gores. Measurement of transference numbers for Lithium ion electrolytes via four different methods, a comparative study. *Electrochimica Acta*, 56(11):3926 – 3933, 2011.
- [76] A. J. Bard and L. R. Faulkner. *Electrochemical Methods: Fundamentals and Applications*. Wiley, New York, 1980.
- [77] Macdonald J.R. *Electrochemical Methods: Fundamentals and Applications*. Wiley, New York, 1987.
- [78] Anders Ferry, Marca M. Doeff, and Lutgard C. De Jonghe. Transport property and raman spectroscopic studies of the polymer electrolyte system P(EO)_n – NaTFSI. *J. Electrochem. Soc.*, 145:1586–1592, 1998.

- [79] Lars Ole Valoen and Jan N. Reimers. Transport properties of LiPF_6 -based Li-ion battery electrolytes. *Journal of The Electrochemical Society*, 152:A882–A891, 2005.
- [80] Andreas Nyman. *An Experimental and Theoretical Study of the Mass Transport in Lithium Ion Battery Electrolytes*. PhD thesis, Ph.D. Thesis, Kungliga Tekniska Hgskolan, 2011.
- [81] Gholam-Abbas Nazri and Gianfranco Pistoia. *Lithium Batteries: Science and Technology*. Springer, 2003.
- [82] Jianwen Yang, Bo Yan, Jing Ye, Xue Li, Yansheng Liua, and Haiping Youa. Carbon-coated licrtio4 electrode material promoting phase transition to reduce asymmetric polarization for Lithium-ion batteries. *Phys. Chem. Chem. Phys.*, 16:2882–2891, 2014.
- [83] Qing Wang, Hong Li, Xuejie Huang, and Liquan Chenz. Determination of chemical diffusion coefficient of Lithium ion in graphitized mesocarbon microbeads with potential relaxation technique. *J. Electrochem. Soc.*, 148:A737–A741, 2001.
- [84] Jian Xie, Nobuyuki Imanishi, Tadaaki Matsumura, Atsushi Hirano, Yashuo Takeda, and Osamu Yamamoto. Orientation dependence of Li-ion diffusion kinetics in licoo2 thin films prepared by rf magnetron sputtering. *Solid State Ionics*, 179:362–370, 2008.
- [85] M. D. Levi and D. Aurbach. Diffusion coefficients of Lithium ions during intercalation into graphite derived from the simultaneous measurements and

- modeling of electrochemical impedance and potentiostatic intermittent titration characteristics of thin graphite electrodes. *J. Phys. Chem. B*, 101:4641–4647, 1997.
- [86] Y.-H. Chen, C.-W. Wang, G. Liu, X.-Y. Song, V. S. Battaglia, and A. M. Sastrya. Selection of conductive additives in Li-ion battery cathodes. a numerical study. *J. Electrochem. Soc.*, 154:A978–A986, 2007.
- [87] Indrajeet V. Thorat. *Understanding performance-limiting mechanisms in Lithium-ion batteries for high-rate applications*. ProQuest, UMI Dissertation Publishing, 2011.
- [88] F. Sauvage, J-M. Tarascon, and E. Baudrin. In situ measurements of li ion battery electrode material conductivity: Application to Li_xCOO_2 and conversion reactions. *J. Phys. Chem. C*, 111:9624–9630, 2007.
- [89] Tiehua Piao, Su-Moon Park, Chil-Hoon Doh, and Seong-In Moonb. Intercalation of Lithium ions into graphite electrodes studied by ac impedance measurements. *Journal of The Electrochemical Society*, 146:2794–2798, 1999.
- [90] John Newman and K. E. Thomas-Alyea. *Electrochemical Systems, 3rd Edition*. Wiley-Interscience, 2004.
- [91] F. Nobile, R. Tempone, and C. G. Webster. A sparse grid stochastic collocation method for partial differential equations with random input data. *SIAM Journal on Numerical Analysis*, 46(5):2309–2345, 2008.

- [92] L. Mathelin and M.Y. Hussaini. A stochastic collocation algorithm for uncertainty analysis. Technical Report NAS 1.26:212153; NASA/CR-2003-212153, NASA Langley Research Center, 2003.
- [93] D. Xiu and J.S. Hesthaven. High-order collocation methods for differential equations with random inputs. *SIAM J. Sci. Comput.*, 27(3):1118–1139, 2005.
- [94] I. Babuška, F. Nobile, and R. Tempone. A stochastic collocation method for elliptic partial differential equations with random input data. Technical Report 05-47, The Institute for Computational Engineering and Sciences (ICES), University of Texas, Austin, 2005. <http://www.ices.utexas.edu/research/reports/2005.php>.
- [95] S. Smolyak. Quadrature and interpolation formulas for tensor products of certain classes of functions. *Soviet Mathematics, Doklady*, 4:240–243, 1963.
- [96] Jan N. Reimers, Mark Shoesmith, Yong Shou Lin, and Lars Ole Valoen. Simulating high current discharges of power optimized Li-ion cells. *J. Electrochem. Soc.*, 160:A1870–A1884, 2013.
- [97] Jan N. Reimers. Accurate and efficient treatment of foil currents in a spiral wound Li-ion cell. *J. Electrochem. Soc.*, 161:A118–A127, 2014.

Nomenclature		Ω	sample set
D	diffusion coefficient of the liquid phase [$\text{m}^{-2} \cdot \text{s}^{-1}$]	α_i	PC coefficients
D_s	diffusion coefficient of the solid phase [$\text{m}^{-2} \cdot \text{s}^{-1}$]	ξ	vector of input random variables
F	Faraday's constant = 97484 [$\text{C} \cdot \text{mol}^{-1}$]	δ	Kronecker delta or Dirac delta function
I	total current density across the stack [$\text{amp} \cdot \text{m}^{-2}$]	ϵ	porosity of electrodes and stack
L	width [m]	η	over-potential in electrodes [V]
N	number of samples	γ	the truncation error tolerance of BPDN problem
P	number of PC basis functions of p th total order in dimension d	κ	electronic conductivity of the liquid phase [$\text{S} \cdot \text{m}^{-1}$]
S_k	first order Sobol' index of k th random input	κ_D	liquid phase diffusional conductivity [$\text{S} \cdot \text{m}^{-1}$]
S_k^T	total Sobol' index of k th random input	brugg	Bruggeman coefficient
T	temperature [K]	$\mathcal{J}_{d,p}$	set of p th order multi-indices in dimension d
V	open circuit potential of the active material [V]	ϕ_{cell}	cell voltage [V]
		ϕ_e	Li^+ ion potential in liquid phase [V]

ϕ_s	electron potential in the solid phase [V]	k	reaction rate constant [$\text{m}^4 \cdot \text{mol} \cdot \text{s}$]
ψ_i	multivariate PC basis functions	p	total order of the PC expansion
$\rho(\xi)$	probability measure of random variable ξ	r	micro-scale distance from the center of solid particle [m]
σ	electronic conductivity of the solid phase [$\text{S} \cdot \text{m}^{-1}$]	r_s	solid particle size [m]
τ	tortuosity	t	time [s]
a	active particle surface area per unit volume of electrode [$\text{m}^2 \cdot \text{m}^{-3}$]	t_+^0	Li^+ transference number
		x	distance from anode [m]

Superscripts

c	salt concentration in liquid phase [$\text{mol} \cdot \text{m}^{-3}$]	eff	effective value
c_s	lithium concentration in solid phase [$\text{mol} \cdot \text{m}^{-3}$]	h	harmonic mean
c_s^{surf}	lithium concentration in solid phase at $r = r_s$ [$\text{mol} \cdot \text{m}^{-3}$]	j	unit flux portion
		o	internal mixing portion

Subscripts

d	number of random inputs	i	multi-index
i_{ex}	exchange current density of an electrode reaction [$\text{amp} \cdot \text{m}^{-2}$]	max	maximum
j_{vol}	volumetric reaction flux in the pore walls [$\text{amp} \cdot \text{m}^{-3}$]	a	anode
		c	cathode
		s	separator